SKELETAL MECHANISM GENERATION FOR SURROGATE FUELS

by

KYLE EVAN NIEMEYER

Submitted in partial fulfillment of the requirements

for the degree of Master of Science in Aerospace Engineering

Thesis advisor: Dr. Chih-Jen Sung

Department of Mechanical and Aerospace Engineering

CASE WESTERN RESERVE UNIVERSITY

January, 2010

CASE WESTERN RESERVE UNIVERSITY

SCHOOL OF GRADUATE STUDIES

We hereby approve the thesis/dissertation of

Kyle Evan Niemeyer

candidate for the Master of Science degree *.

(signed) Prof. Chih-Jen Sung
(chair of the committee)

Prof. James S. T'ien

Prof. J. Iwan D. Alexander

Dr. Mandhapati P. Raju

(date) 09/19/2009

*We also certify that written approval has been obtained for any proprietary material contained therein.

Copyright © 2009 Kyle Evan Niemeyer

This work is licensed by the author under a
Creative Commons Attribution-Noncommercial-No Derivative Works 3.0 License
http://creativecommons.org/licenses/by-nc-nd/3.0/us/

Contents

Table of Contents 1

List of Tables 3

List of Figures 4

Acknowledgements 6

List of Abbreviations 7

Abstract 9

1 Introduction 11

1.1 Motivation 11

1.2 Mechanism Reduction 13

1.2.1 Time-scale Reduction Methods 14

1.2.2 Skeletal Reduction Methods 14

1.3 Directed Relation Graph-based Methods 16

1.4 Chapter Breakdown 18

2 Mechanism Automatic Reduction Software (MARS) 19

2.1 Overview 19

2.2 Data Sampling 21

2.3 DRGEP Phase 23
2.4 Sensitivity Analysis Phase 27

3 Results and Discussion **29**
3.1 *n*-Heptane 29
3.1.1 Preliminary *n*-Heptane Skeletal Reduction 30
3.1.2 Comprehensive *n*-Heptane Skeletal Reduction 34
3.2 *iso*-Octane 39
3.3 *n*-Decane 42
3.4 Discussion 50

4 Conclusions and Future Work **51**

Appendices **55**

Appendix A *n*-Heptane Comprehensive Skeletal Mechanism **56**

Appendix B *iso*-Octane Comprehensive Skeletal Mechanism **58**

Appendix C *n*-Decane Comprehensive Skeletal Mechanism **60**

Appendix D *n*-Decane High-Temperature Skeletal Mechanism **63**

Bibliography **64**

List of Tables

3.1 Comparison of *n*-heptane skeletal mechanism sizes generated by DRG, DRGEP, DRGASA, and DRGEPSA methods. 35

3.2 Comparison of sensitivity analysis results using DRGASA and DRGEPSA methods. 38

3.3 Comparison of *iso*-octane skeletal mechanism sizes generated by DRG, DRGEP, DRGASA, and DRGEPSA methods. 41

3.4 Summary of *n*-decane skeletal mechanism results. 43

List of Figures

1.1 A simple directed graph showing species coupling and dependent sets. 17

2.1 Flowchart illustrating MARS program inputs and components, as well as future additions. 20

2.2 An example of the temperature and pressure data points sampled during the ignition evolution used in the chemical kinetics analysis. . . . 22

2.3 A directed relation graph showing path-dependent species coupling. . 25

3.1 Number of species as a function of error limit for skeletal mechanisms for n-heptane generated using DRG, DRGEP, DRGASA, and DRGEPSA in the MARS implentation. 31

3.2 Number of species and maximum error of skeletal mechanisms for n-heptane generated by DRG using various threshold values (ε_{DRG}). . . 32

3.3 Number of species and maximum error of skeletal mechanisms for n-heptane generated by DRGEP using various threshold values (ε_{EP}). . 33

3.4 Autoignition validation of n-heptane skeletal mechanisms over a range of initial temperatures and pressures, and at varying equivalence ratios. 36

3.5 Induced error in ignition delay versus OIC values for species considered with sensitivity analysis phase in DRGEPSA during the n-heptane reduction. 37

3.6 Autoignition validation of *iso*-octane skeletal mechanisms over a range of initial temperatures and pressures, and at varying equivalence ratios. 40
3.7 Autoignition validation of comprehensive *n*-decane skeletal mechanism (202 species and 846 reactions) over a range of initial temperatures and pressures, and at varying equivalence ratios. 44
3.8 Autoignition validation of *n*-decane high-temperature skeletal mechanism over a range of initial temperatures and pressures, and at varying equivalence ratios. 45
3.9 PSR validation of comprehensive *n*-decane skeletal mechanism (202 species and 846 reactions) over a range of residence times and at varying pressures and equivalence ratios with an inlet temperature of 300 K. 46
3.10 PSR validation of *n*-decane high-temperature skeletal mechanism over a range of residence times and at varying pressures and equivalence ratios with an inlet temperature of 300 K. 47
3.11 Laminar flame speed validation of comprehensive *n*-decane skeletal mechanism (202 species and 846 reactions) over a range of equivalence ratio and pressure conditions with an unburned mixture temperature of 400 K. 48
3.12 Laminar flame speed validation of *n*-decane high-temperature skeletal mechanism over a range of equivalence ratio and pressure conditions with an unburned mixture temperature of 400 K. 49

Acknowledgements

I would like to thank Dr. Chih-Jen Sung for providing me with the opportunity to pursue graduate education in a field that truly interests me and for his continuing support and instruction.

I would also like to thank Dr. Mandhapati P. Raju for his work in starting this project and Dr. Kamal Kumar and the other members of the Combustion Diagnostics Laboratory for their advice and support.

Additionally, I would like to acknowledge funding from the National Aeronautics and Space Administration under Grant No. NNX07AB36Z, with the technical monitoring of Dr. K. P. Kundu, and the Department of Defense through the National Defense Science and Engineering Graduate (NDSEG) Fellowship program.

Lastly, I would like to thank my family, who have supported me throughout my life and education, and Bryony, who has given me emotional support through all of this.

List of Abbreviations

QSS	—	Quasi-Steady State
CSP	—	Computational Singular Perturbation
DRG	—	Directed Relation Graph
DRGEP	—	Directed Relation Graph with Error Propagation
DRGASA	—	Directed Relation Graph-aided Sensitivity Analysis
SA	—	Sensitivity Analysis
S_k	—	the kth chemical species
$[S_k]$	—	the concentration of the kth chemical species
n_S	—	total number of species in reaction mechanism
n_R	—	total number of elementary reactions in reaction mechanism
$\nu'_{k,i}$	—	stoichiometric coefficient of reactant species k in reaction i
$\nu''_{k,i}$	—	stoichiometric coefficient of product species k in reaction i
$\nu_{k,i}$	—	overall stoichiometric coefficient of species k in reaction i
$\omega_{\mathrm{f},i}$	—	forward reaction rate of reaction i
$\omega_{\mathrm{r},i}$	—	reverse reaction rate of reaction i
ω_i	—	overall reaction rate of reaction i
$\dot{\omega}_k$	—	production rate of species k
$k_{\mathrm{f},i}$	—	forward reaction rate constant of reaction i
$k_{\mathrm{r},i}$	—	reverse reaction rate constant of reaction i
$K_{\mathrm{c},i}$	—	equilibrium constant of reaction i

r_{AB}^{DRG}	—	DRG direct interaction coefficient
r_{AB}	—	Direct Interaction Coefficient (DIC)
$r_{AB,p}$	—	Path-dependent Interaction Coefficient (PIC)
R_{AB}	—	Overall Interaction Coefficient (OIC)
$\varepsilon_{\mathrm{DRG}}$	—	DRG error threshold
$\varepsilon_{\mathrm{EP}}$	—	DRGEP error threshold
ε^*	—	DRGEPSA upper error threshold
ϕ	—	Equivalence ratio

Skeletal Mechanism Generation for Surrogate Fuels

Abstract

by

KYLE EVAN NIEMEYER

The Mechanism Automatic Reduction Software (MARS) implementation for chemical reaction mechanism reduction, with special emphasis on skeletal reduction using the directed relation graph with error propagation and sensitivity analysis (DRGEPSA), is developed and demonstrated with examples for three hydrocarbon components, *n*-heptane, *iso*-octane, and *n*-decane, relevant to surrogate fuel development. DRGEPSA integrates two previously developed methods, directed relation graph-aided sensitivity analysis (DRGASA) and directed relation graph with error propagation (DRGEP), by first applying DRGEP to efficiently remove many unimportant species prior to sensitivity analysis to further remove unimportant species, producing an optimally small skeletal mechanism for a given error limit. It is illustrated that the combination of the DRGEP and DRGASA methods allows the DRGEPSA approach to overcome the weaknesses of each, specifically that DRGEP cannot identify all unimportant species and that DRGASA shields unimportant species from removal. Skeletal mechanisms for *n*-heptane and *iso*-octane generated using the DRGEP, DRGASA, and DRGEPSA methods are presented and compared to illustrate the improvement of DRGEPSA. Two skeletal mechanisms for *n*-decane generated using DRGEPSA, one covering a comprehensive range of temperature, pressure, and equivalence ratio con-

ditions for autoignition and the other limited to high temperatures, are presented and validated. Both mechanisms are further demonstrated to well reproduce the results of the detailed mechanism in perfectly-stirred reactor and laminar flame simulations over a wide range of conditions.

Chapter 1

Introduction

1.1 Motivation

Combustion of hydrocarbon fuels currently provides 85% of the energy produced in the United States [1, 2]. Transportation accounts for approximately 30%, of which 97% derives from petroleum [1]. Due to the dwindling worldwide supply and the location of the major remaining sources in unstable regions of the world, decreasing fuel consumption and expanding energy sources are national priorities. Additionally, there are major worldwide concerns about emissions including pollutants, such as NO_x, SO_x, and soot, and greenhouse gases such as CO_2. Diverse alternative options exist such as nuclear and renewable sources of energy and are being pursued to supplement and eventually replace traditional combustion-based sources, but hydrocarbon will remain the major component for the next few decades. With this in mind, there is considerable demand to improve efficiency to decrease consumption and reduce emissions for the next generation combustion technology. Efficiency improvements due to advanced fuel and engine concepts could account for 25–50% reduction in fuel usage [1] and recent developments such as homogeneous compression charge ignition (HCCI) engines offer the potential of significantly reduced emissions [3]. Fuel-flexible

designs that can use both conventional and alternative fuels are also desired to diversify consumption.

Computational modeling drives the design of engines and combustors for aerospace, transportation, and energy applications. Recent advancements in Reynolds-Averaged Navier–Stokes and Large Eddy Simulation combustion modeling allow simulation of realistic devices. For instance, development of advanced concepts in solid rocket engines, pulse combustion, and direct injection and HCCI internal combustion engines rely almost exclusively on modeling [3]. Historically, practical combustion simulations used one- or multi-step semiglobal reactions to enable the inclusion of chemical kinetics. While such simplifications are adequate for equilibrium problems, in addition to neglecting many species and radicals they do not adequately predict combustion phenomena over wide ranges of conditions [4]. Accurate prediction of fuel combustion and pollutant emissions requires comprehensive detailed reaction mechanisms.

Detailed reaction mechanisms for hydrogen and hydrocarbons typically contain tens to thousands of species and hundreds to thousands of reactions. For instance, a detailed mechanism for hydrogen contains 11 species and 19 reactions [5], while a standard mechanism for methane/natural gas, GRI-Mech 3.0, contains 53 species and 325 reactions [6]. The size of detailed mechanisms in general increases with the number of carbon atoms. Liquid transportation fuels contain varying blends of many large hydrocarbons. There has been a recent collaborative effort to develop surrogate models to emulate real fuels to accurately predict combustion properties. Such surrogate models typically contain mixtures of a small number of appropriate liquid hydrocarbons. Simple surrogates of gasoline contain *iso*-octane alone, while binary blends consist of *n*-heptane and *iso*-octane (the primary reference fuels for octane ratings). More complex surrogates contain toluene and many more species; highly detailed surrogate mechanisms can contain more than 1000 species and 4000–10000 reactions [7, 8]. Surrogates for diesel [8, 9] and jet fuels [10–12] also contain large num-

bers of species and reactions. For instance, a recently developed detailed mechanism for $C_8 - C_{16}$ *n*-alkane hydrocarbons, important surrogate components, contains 2115 species and 8157 reactions [13], while a mechanism for methyl-decanoate, a biodiesel surrogate, contains 2878 species and 8555 reactions [14].

Despite rapid advancements in computing power in recent years, it is generally formidable to integrate such detailed reaction mechanisms into large-scale computational simulations in terms of CPU time and memory requirements. Since the computational cost of chemistry scales by the third power of the number of species [15], such large sizes pose problems even in zero-dimensional modeling. In addition, the wide range of time scales (from nanosecond to second) and the nonlinear coupling between species and reactions induces stiffness when governing equations are solved [15]. Due to these computational demands, reduction of large mechanisms is necessary to facilitate practical simulations using realistic chemistry with modern computational tools.

1.2 Mechanism Reduction

Much effort has been dedicated to the development of effective skeletal reduction techniques, as reviewed by Griffiths [16], Tomlin et al. [17], and Okino and Mavrovouniotis [18]. There are two major types of mechanism reduction: skeletal reduction, the elimination of unimportant species and/or reactions to decrease the size of the mechanism, and reduction based on time-scale analysis to diminish the stiffness. The current work is focused on skeletal reduction but major time-scale reduction methods are first described for completeness and their relation to future work.

1.2.1 Time-scale Reduction Methods

The quasi-steady state (QSS) [19, 20] and partial equilibrium (PE) [21, 22] assumptions are two classical methods based on time-scale analysis used to reduce the number of variables in a differential reacting system. By assuming QSS species achieve a quasi-steady state after an initial fast transient, algebraic relations with the other species in the reaction system replace differential equations for the concentrations of the QSS species. Similarly, the PE approximation assumes reactions achieve partial equilibrium after a transient period. The Computer Assisted Reduction Method developed by Chen [23] provides a simple automated methodology to reduce the number of differential variables based on given QSS species. Recently, the QSS and PE approximations were used to remove stiffness on-the-fly [24]. Systematic methods of time-scale analysis include intrinsic low dimensional manifolds [25, 26] and computational singular perturbation (CSP) [27–29] which use Jacobian analysis to decouple the fast and slow modes. Concepts involved in these approaches can also be used to identify QSS species and PE reactions [30, 31].

1.2.2 Skeletal Reduction Methods

Skeletal reduction is typically the first step of mechanism reduction, where species and reactions deemed negligible to important phenomena over the range of conditions of interest (e.g., pressure, temperature, and equivalence ratio) are removed from the detailed mechanism. Methods include lumping [32–34], genetic algorithms [35, 36], optimization [37–39], and adaptive reduction approaches [40–44]. Particularly relevant methods are described briefly here.

Sensitivity analysis (SA) [45–47] is a classical method that analyzes the Jacobian matrix to identify and eliminate unimportant species and reactions. Principal component analysis [48, 49] was introduced as an improvement to SA that provides some information about the interaction of species and reactions through eigendecompo-

sition of the sensitivity matrix. While these methods provide definitive information about the importance of species and reactions, the use of expensive Jacobian and sensitivity matrix calculations prohibits exclusive use in the large reactions mechanisms currently of interest. The detailed reduction method [50] provides a significantly less computationally expensive approach that compares reaction rates to a critical value. Slower reactions are not necessarily less important than fast reactions, however, and the selection of the critical reaction rate is highly situation-dependent and therefore limits the general applicability of this method.

Time-scale analysis methods can be employed to perform skeletal reduction as well. CSP-based methods [51–53] analyze the Jacobian matrix to decompose species relations into fast and slow components. Species are considered important if coupling is strong in either the fast or slow subspace. This approach can overestimate the importance of some species, however, and produce skeletal mechanisms of larger size than other methods [54]. Another method similar to CSP is level of importance (LOI) analysis [40, 55–57], which combines time scale analysis with sensitivity analysis to rank species importance. The most recent work [57] using LOI presented skeletal mechanisms for ethylene that are competitive with those generated using other methods [58] though the range of conditions considered in the LOI analysis was much narrower.

The chemistry-guided reduction (CGR) [59] approach was recently presented and applied to a detailed mechanism for n-heptane [60]. This method combines lumping and necessity analysis applied to a compact starting mechanism. Though the resulting mechanism sizes are competitive with those from other methods (and the current work), CGR is not explicitly error-controlled and the emphasis on a small starting mechanism could be a possible limitation of the method.

Nagy and Turányi [61] developed the simulation error minimization connectivity method, based on the original connectivity method proposed by Turányi [47], which

exhaustively analyzes sets of important species through Jacobian analysis and selects an optimal mechanism based on an error limit. The method was shown to provide minimal mechanism sizes for a given error but at a computational expense an order of magnitude above other methods [61]. This could limit the applicability of the approach to the particularly large mechanisms considered in the current work.

Recently, a skeletal reduction method based on graph theory called the directed relation graph (DRG) received much attention. This method is the basis for the current work and is described in detail in Section 1.3.

1.3 Directed Relation Graph-based Methods

When solving the chemical kinetics of a detailed reaction mechanism, the elementary reactions are treated as:

$$\sum_{k=1}^{n_S} \nu'_{k,i} S_k \rightleftharpoons \sum_{k=1}^{n_S} \nu''_{k,i} S_k \quad i = 1, ..., n_R, \tag{1.1}$$

where the overall reaction rate of each reaction is

$$\omega_i = \omega_{f,i} - \omega_{r,i} \tag{1.2}$$

$$= k_{\mathrm{f},i} \prod_{k=1}^{n_S} [S_k]^{\nu'_{k,i}} - k_{\mathrm{r},i} \prod_{k=1}^{n_S} [S_k]^{\nu''_{k,i}} \tag{1.3}$$

and where

$$k_{\mathrm{r},i} = \frac{k_{\mathrm{f},i}}{K_{\mathrm{c},i}}. \tag{1.4}$$

The production rate of each species S_k can be expressed as

$$\dot{\omega}_k = \sum_{i=1}^{n_R} \nu_{k,i} \omega_i, \tag{1.5}$$

where $\nu_{k,i} = \nu''_{k,i} - \nu'_{k,i}$ is the net stoichiometric coefficient for species k in reaction i.

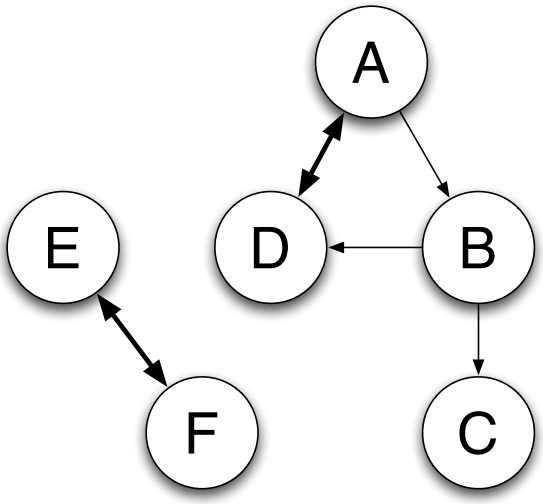

Figure 1.1: A simple directed graph showing species coupling and dependent sets.

The DRG method, originally proposed by Lu and Law [54, 58, 62], uses a directed graph to map the coupling of species and consequently find unimportant species for removal. The reaction system is mapped according to the following rules: (1) each vertex represents a unique species, (2) there is a directed edge from species A to species B if $r_{AB}^{\mathrm{DRG}} \geq \varepsilon_{\mathrm{DRG}}$, where

$$r_{AB}^{\mathrm{DRG}} = \frac{\sum_{i=1}^{n_R} |\nu_{A,i}\omega_i\delta_B^i|}{\sum_{i=1}^{n_R} |\nu_{A,i}\omega_i|} \tag{1.6}$$

$$\delta_B^i = \begin{cases} 1, & \text{if the } i\text{th elementary reaction involves species B;} \\ 0, & \text{otherwise,} \end{cases} \tag{1.7}$$

and $\varepsilon_{\mathrm{DRG}}$ is an error threshold (e.g., 0.1), and (3) the starting vertices of the DRG are key species in the mechanism. A depth-first search initiates at the starting vertices to find necessary species; species reached by the search are considered important and retained in the skeletal mechanism. Figure 1.1 shows a simple directed graph illustrating the dependence of species in the direction of the directed edges. For instance, species A depends of species B but the dependence is not symmetric. Thicker directed edges represent stronger dependence between species pairs.

Further development of the DRG method branched into two major directions: (1) DRG-aided sensitivity analysis (DRGASA) [63, 64], from the original authors of the DRG method which performs sensitivity analysis on species not removed by DRG to further reduce the mechanism, and (2) DRG with error propagation (DRGEP) [65], which considers the propagation of error due to species removal down reaction pathways. Another method based on DRG, path flux analysis [66], was recently presented that uses production and consumption fluxes to identify important reaction pathways. DRGEP and DRGASA are discussed in more detail in Chapter 2, as the current skeletal reduction approach integrates the major aspects of DRGEP and DRGASA into DRG with error propagation and sensitivity analysis (DRGEPSA). The objective of this combined approach is to overcome the weaknesses of the two individual methods, as is demonstrated. The DRGEPSA method was initially presented by Raju et al. [67] and more recently by Niemeyer et al. [68, 69].

1.4 Chapter Breakdown

In Chapter 2, the Mechanism Automatic Reduction Software (MARS) implementation and DRGEPSA methodology is described in detail. In Chapter 3, skeletal mechanisms for n-heptane and *iso*-octane generated using DRG, DRGASA, DRGEP, and DRGEPSA are presented to compare the various methods. Two skeletal mechanisms for n-decane, generated using DRGEPSA, are also presented and validated. Finally, conclusions and suggestions for future work are discussed in Chapter 4.

Chapter 2

Mechanism Automatic Reduction Software (MARS)

2.1 Overview

MARS is designed to integrate chemical kinetics sampling and automatic mechanism reduction into a single computer program that requires minimal user input and interaction. The required inputs to generate a skeletal mechanism are limited to the starting detailed mechanism, the desired range of conditions (e.g., temperature, pressure, equivalence ratio) of validity for the skeletal mechanism, and the maximum error tolerance. In addition, optimization of skeletal mechanisms requires the secondary inputs of target species and the upper threshold but the end user need not be aware of these. By requiring few, simple inputs, the program is accessible to users with limited experience in mechanism reduction or even reacting flow/combustion modeling.

The program is coded in FORTRAN 77/Fortran 90 and uses CHEMKIN-III [70] to interpret the detailed mechanism and handle the chemical kinetics. First, zero-dimensional simulations are performed to sample data and to generate baseline results from which the error of skeletal mechanisms are found. Following this, the

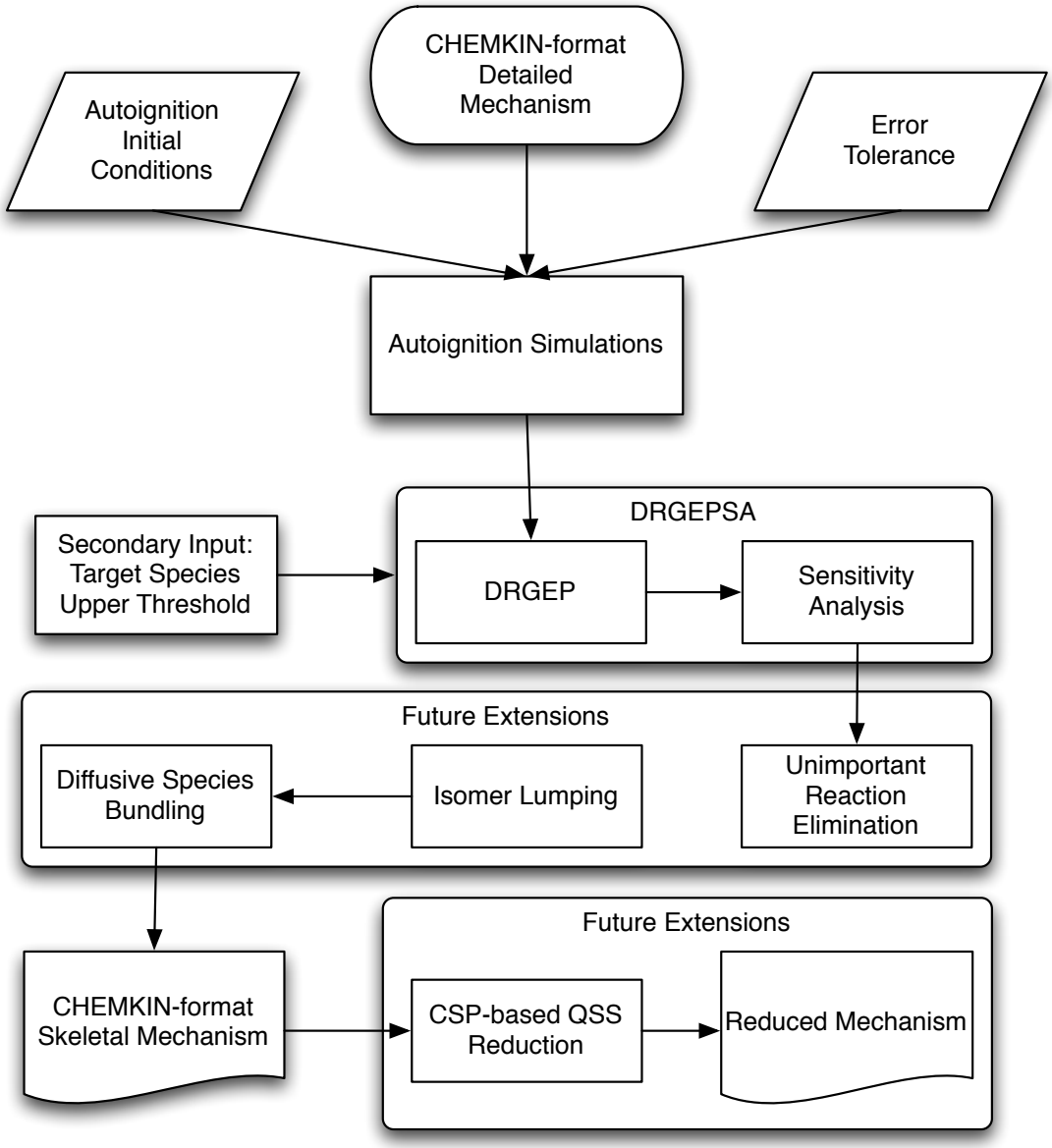

Figure 2.1: Flowchart illustrating MARS program inputs and components, as well as future additions.

DRGEP method efficiently identifies and removes unimportant species. The optimal DRGEP threshold is found iteratively by generating skeletal mechanisms using various threshold values and finding the error with respect to the detailed mechanism. This produces a minimal mechanism using DRGEP for the given error limit prior to using computationally-expensive sensitivity analysis. The remaining species are then separated into two groups using the overall interaction coefficients (OICs) calculated in DRGEP: (1)"limbo" species for sensitivity analysis and (2) important species for automatic retention. Sensitivity analysis performed on limbo species then identifies further unimportant species which are removed until the global error reaches the given limit. At all steps of the procedure, reactions containing eliminated species are also removed from the mechanism. See Fig. 2.1 for a flowchart illustrating the steps of the MARS implementation as well as future additions to the mechanism reduction procedure; specifically, extensions such as unimportant reaction elimination, isomer lumping, diffusive species bundling, and CSP-based QSS reduction will be pursued.

2.2 Data Sampling

The current implementation begins with simulations of constant volume autoignition using SENKIN [71] with the detailed reaction mechanism. The user-provided range of initial conditions, along with the error limit, determines the range of conditions (temperature, pressure, equivalence ratio) over which the resulting skeletal mechanism is valid. The chemical kinetics data are sampled densely at 18 points during the ignition evolution, as illustrated by Fig. 2.2, and are used for the subsequent analysis. Additionally, the ignition delay results are stored to later measure the global error of skeletal mechanisms generated during the reduction process.

I propose that using constant volume autoignition for the reduction procedure provides adequate data to generate a valid skeletal mechanism. This requires exter-

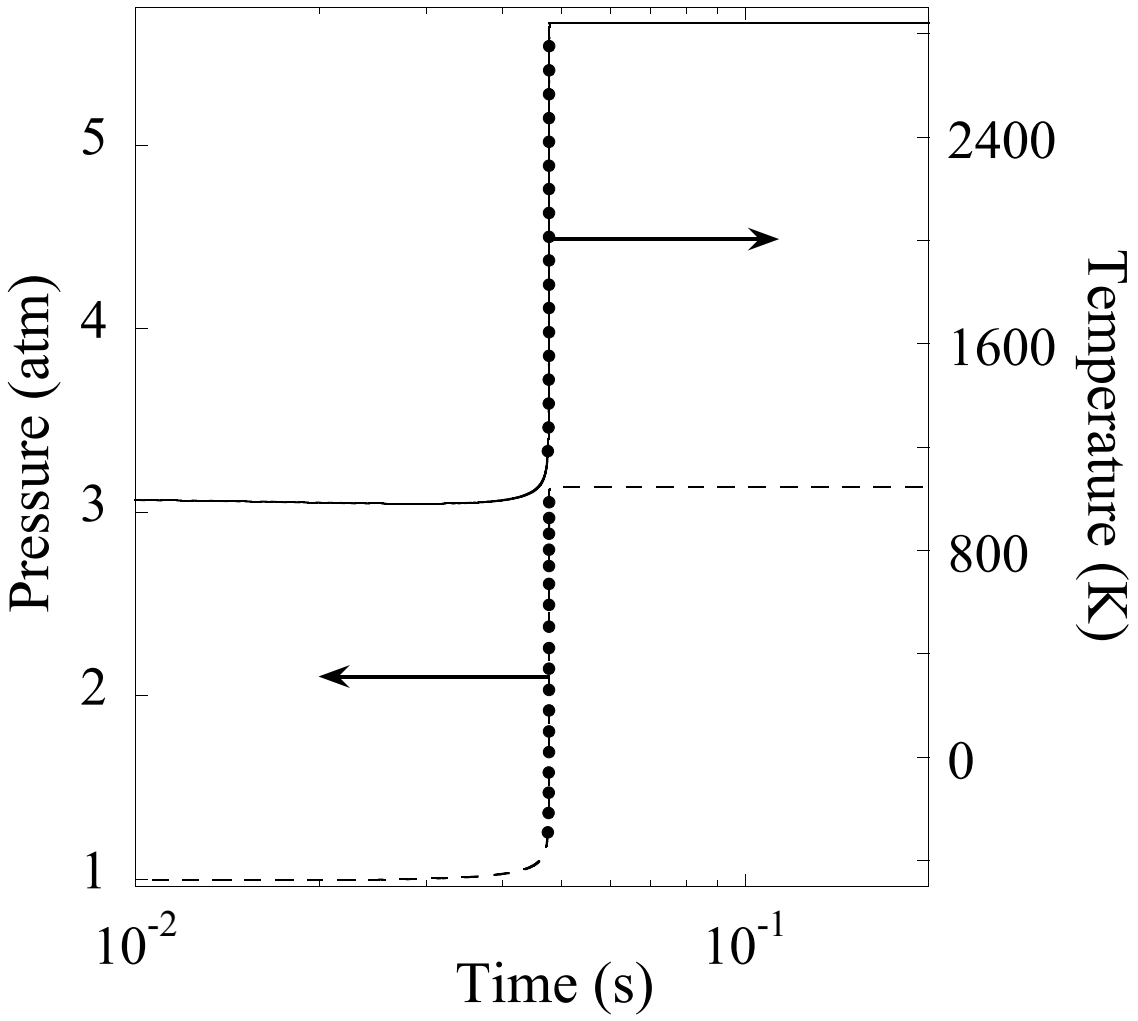

Figure 2.2: An example of the temperature and pressure data points sampled during the ignition evolution used in the chemical kinetics analysis.

nal validation using other types of combustion simulations to determine the general validity of skeletal mechanisms produced in this manner. The MARS framework, however, provides for simple expansion to include other such simulations should it be desired.

2.3 DRGEP Phase

The first phase of DRGEPSA is based on the DRGEP of Pepiot-Desjardins and Pitsch [65], which in turn is an extension of the original DRG of Lu and Law [54, 58, 62]. The current DRGEP implementation includes an improved definition of the direct interaction coefficient motivated by the shortcomings of the original definition [72] in situations with long chemical paths involving fast modes [54]. The DRGEP approach uses a directed relation graph to map the coupling of species in a reaction system, where the vertices represent species and directed edges between vertices represent the coupling of species. The dependence of one species on another is based on a contribution to overall production or consumption rate. Therefore the accurate prediction of the production of a species A that is strongly dependent on another species B requires the presence of species B in the reaction mechanism. This dependence is not necessarily symmetric, as species A may interact with many more or less species than species B, for instance. This contribution is expressed with the DRGEP interaction coefficient (DIC):

$$r_{AB} = \frac{\left|\sum_{i=1}^{n_R} \nu_{A,i}\omega_i\delta_B^i\right|}{\max\left(P_A, C_A\right)}, \tag{2.1}$$

where

$$P_A = \sum_{i=1}^{n_R} \max\left(0, \nu_{A,i}\omega_i\right), \tag{2.2}$$

$$C_A = \sum_{i=1}^{n_R} \max\left(0, -\nu_{A,i}\omega_i\right), \tag{2.3}$$

$$\delta_B^i = \begin{cases} 1, & \text{if the } i\text{th elementary reaction involves species B;} \\ 0, & \text{otherwise,} \end{cases} \tag{2.4}$$

A and B represent the species of interest (with dependency in the $A \rightarrow B$ direction) and i is the ith reaction. The DIC is an estimate for the error in the overall production of species A induced by the removal of species B.

The error propagation concept is introduced with the definition of the path-dependent interaction coefficient (PIC). After mapping the reaction system, a depth first search is performed starting at the target species (in general fuel, oxidizer, important radicals or pollutants) to find the dependency pathways for all species relative to the targets. A PIC represents the error propagation down a certain pathway and is defined as the product of intermediate DICs between the target A and species of interest B down a certain path in the directed graph:

$$r_{AB,p} = \prod_{k=1}^{n-1} r_{S_k S_{k+1}}, \tag{2.5}$$

where n is the number of species between A and B in pathway p and S is a placeholder for the intermediate species starting at species A and ending at species B. The overall interaction coefficient (OIC) is then defined as the maximum of all PICs between the targets and all other species:

$$R_{AB} = \max_{\text{all paths } p} \left(r_{AB,p}\right). \tag{2.6}$$

For example, Fig. 2.3 shows a simple reaction system where the overall dependence of species A on species D based on DRG and DRGEP are respectively expressed as:

$$R_{AD}^{\text{DRG}} = \max\left(r_{AB}, r_{BD}, r_{AC}, r_{CD}, r_{CE}, r_{ED}\right)$$

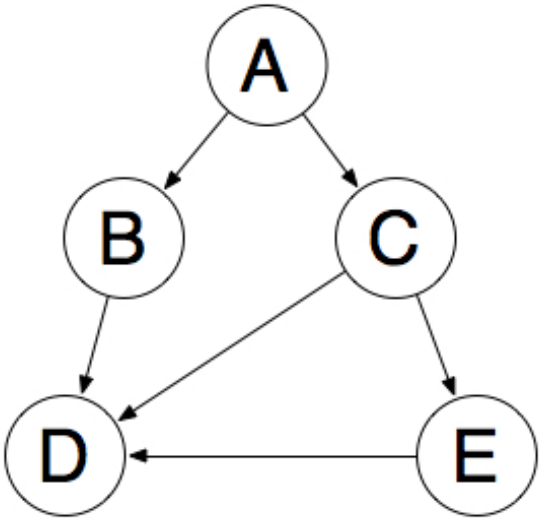

Figure 2.3: A directed relation graph showing path-dependent species coupling.

and

$$R_{AD}^{\mathrm{DRGEP}} = \max\left(r_{AD,1}, r_{AD,2}, r_{AD,3}\right),$$

where path one is $A \rightarrow B \rightarrow D$, path two is $A \rightarrow C \rightarrow D$, and path three is $A \rightarrow C \rightarrow E \rightarrow D$ such that

$$r_{AD,1} = r_{AB} \cdot r_{BD}, \quad r_{AD,2} = r_{AC} \cdot r_{CD}, \quad r_{AD,3} = r_{AC} \cdot r_{CE} \cdot r_{ED}.$$

The maximum OIC for each species-target pair is used such that each species is assigned a single OIC for the reaction state being considered.

This procedure is performed at each sample point for all kinetics data and the maximum OIC value of all reaction states is used. This concept can be utilized in dynamic reduction where DRGEP is performed at each grid point and time step. Liang et al. [73, 74] recently presented such an approach, dynamic adaptive chemistry (DAC), applied to autoignition and HCCI simulations with very good simulation time reduction. This scheme does not benefit from the sensitivity analysis extension discussed in the current work, however.

The removal of species with OICs below a threshold ε_{EP} is considered negligible to the overall production/consumption of the target species and therefore by the DRGEP theory such species are unimportant for the given conditions and can be removed from the reaction mechanism. The optimal threshold to remove the most unimportant species for a given error limit is chosen in an iterative manner in this DRGEP implementation. A preliminary skeletal mechanism is generated using an initially low ε_{EP} (e.g., 0.01) and the error in ignition delay prediction (compared to the detailed mechanism) is calculated for all initial conditions using the following:

$$\delta_{\text{skel}} = \max_{k \in \mathcal{D}} \frac{\left| \tau^k_{\text{det}} - \tau^k_{\text{skel}} \right|}{\tau^k_{\text{det}}} \tag{2.7}$$

where τ^k_{det} and τ^k_{skel} are the ignition delay results of the detailed and skeletal mechanisms, respectively, and $\mathcal{D}$ is the set of autoignition initial conditions. If the maximum error for this initial skeletal mechanism is above the error limit, the threshold is decreased. For this and any subsequent mechanism, if the maximum error is below the error limit the threshold is increased until the error reaches the specified limit. This procedure generates a minimal skeletal mechanism using DRGEP for a given error limit before sensitivity analysis is performed. This routine could stop prematurely, however, because the relationship between the OICs and global error is in general not linear or even monotonic, which is shown in due course. A smarter iterative method could produce a better initial mechanism but the sensitivity analysis phase should eliminate any unimportant species missed by DRGEP at a greater computational cost, though a better algorithm could make the entire DRGEPSA implementation less computationally expensive.

Proper selection of target species for the DRGEP phase is an important consideration. Unlike in the DRG method, where distance from targets is not taken into account and species only need to be selected to ensure the directed graph is populated

by all species [58, 62], the OIC values used in DRGEP consider species further from targets less important. Careful selection of target species important to the chemical processes of interest can provide greater reduction in DRGEP by better aligning the OIC values with error in global phenomena (e.g., ignition delay, laminar flame speed). Liang et al. [73] performed some analysis of target selection for homogeneous charge compression ignition (HCCI) combustion of *n*-heptane, but the topic merits further study for general applications. In the current work, using the hydrocarbon parent fuel, oxygen, and nitrogen as targets worked well, though additionally including the hydrogen radical for the *n*-heptane and *iso*-octane reductions resulted in slightly smaller final DRGEP and DRGEPSA skeletal mechanisms.

2.4 Sensitivity Analysis Phase

The second phase of DRGEPSA is based on the brute-force sensitivity analysis of Zheng et al. [63]. In particular, species with OIC values that satisfy $\varepsilon_{EP} \leq R_{AB} < \varepsilon^*$, where ε^* is a higher value (e.g., 0.2–0.4), are classified as "limbo" species to be analyzed for removal. Species where $R_{AB} \geq \varepsilon^*$ are classified as retained species and are automatically included in the final skeletal mechanism without further analysis.

Limbo species are first removed from the mechanism one-by-one to find the resulting error in ignition delay induced by the removal, then assigned an error measure:

$$\delta_B = |\delta_{B,\text{ind}} - \delta_{\text{DRGEP}}| \tag{2.8}$$

where $\delta_{B,\text{ind}}$ is the induced error due to the removal of species B with respect to the detailed mechanism and δ_{DRGEP} is the error of the DRGEP-generated mechanism. The limbo species are then sorted in ascending order for removal based on δ_B. Sorting the species in this manner rather than using the induced error, $\delta_{B,\text{ind}}$, alone assures the least important species are removed first. Using induced errors alone for species

ranking would not correctly capture the sensitivity of the species with respect to the baseline DRGEP-generated skeletal mechanism. Species with a $\delta_{B,\text{ind}}$ above the specified error limit are removed from the limbo species list and retained in the final mechanism. The limbo species are then removed from the mechanism in order and the global error is evaluated after each removal. The skeletal reduction is complete when the maximum error reaches the user-specified error limit.

As shown by Turányi [47], a brute-force sensitivity analysis such as the approach used here does not predict the elimination of species groups. Removing many low-error species could induce a larger, unpredictable error greater than the error limit and prematurely end the reduction procedure. To avoid this, the results from sensitivity analysis could be combined with the group-based direct interaction coefficients of the DRGEP implementation of Pepiot-Desjardins and Pitsch [65]. This idea warrants future investigation.

Additionally, a smarter ε^* selection needs to be investigated. MARS currently uses 0.2 for DRGEPSA, based on experience, and 0.4 for DRGASA, based on the value used in previous studies [63, 64]. When a higher value is used in DRGEPSA, a slightly smaller final mechanism can be produced at the expense of mechanism quality in external validation. This is due to the unclear relationship between OIC and induced error in limbo species, as demonstrated in Section 3.1.

Chapter 3

Results and Discussion

3.1 *n*-Heptane

n-Heptane is an important primary reference fuel (PRF) for gasoline with a zero octane number and is also important to diesel studies with a cetane number similar to conventional diesel fuel [7, 9, 75]. Skeletal mechanisms from the detailed mechanism for *n*-heptane of Curran et al. [75, 76], containing 561 species and 2539 reactions, were generated using DRG, DRGASA, DRGEP, and DRGEPSA in the MARS implementation to study the individual weaknesses of the DRGASA and DRGEP methods and the subsequent improvement of the combined method. The DRG and DRGEP methods were performed as the first step of DRGASA and DRGEPSA, respectively. All the methods used the same autoignition chemical kinetics data and the iterative procedure described in Section 2.3 to determine the optimal error threshold values (ε_{DRG} for DRG and DRGASA and ε_{EP} for DRGEP and DRGEPSA). Oxygen, nitrogen, *n*-heptane, and the hydrogen radical were selected as target species for all reduction methods. As discussed earlier, the hydrogen radical was included to increase the extent of reduction for DRGEP and DRGEPSA for the given error limit. The DRG and DRGASA results were not affected by this inclusion because the DRG approach does

not consider distance from targets in the directed graph and the hydrogen radical was already included in the dependent set. First, skeletal mechanisms were generated using limited initial conditions at a wide range of error limits to demonstrate the trends of the various methods. Second, a single error limit was used over a comprehensive range of initial conditions to study in detail the skeletal mechanisms generated by each method.

3.1.1 Preliminary *n*-Heptane Skeletal Reduction

Skeletal mechanisms were generated using DRG, DRGASA, DRGEP, and DRGEPSA to study the trends of the resulting mechanism sizes given various error limits. For illustration, only three constant volume autoignition initial conditions, at 1000 K, 1 atm, and equivalence ratios of 0.5, 1.0, and 1.5, are used to generate the chemical kinetics data and provide error measures. Error limits from 0.5–40% are used to compare the methods. Figure 3.1 shows the numbers of species in the resulting skeletal mechanisms as a function of error limit. It is clear that DRGEPSA produces smaller size skeletal mechanisms for the full range of error limits, while DRGEP and DRGASA produce mechanisms of similar sizes. This is analyzed in greater detail in Section 3.1.2 at a single error limit for a wider range of initial conditions. Another interesting trend appears when comparing the skeletal mechanisms resulting from the methods that include sensitivity analysis. DRGASA and DRGEPSA produce noticeable smaller skeletal mechanisms even at very strict error limits below 3%. This is due to a large number of species with negligible induced error that are in general not well identified by DRG or DRGEP. The reason for this is not yet understood and will be the subject of future study.

To analyze DRG and DRGEP in greater detail, Figs. 3.2 and 3.3 show number of species and maximum error of skeletal mechanisms generated by DRG and DRGEP, respectively, at various error thresholds (ε_{DRG} for DRG and ε_{EP} for DRGEP). As

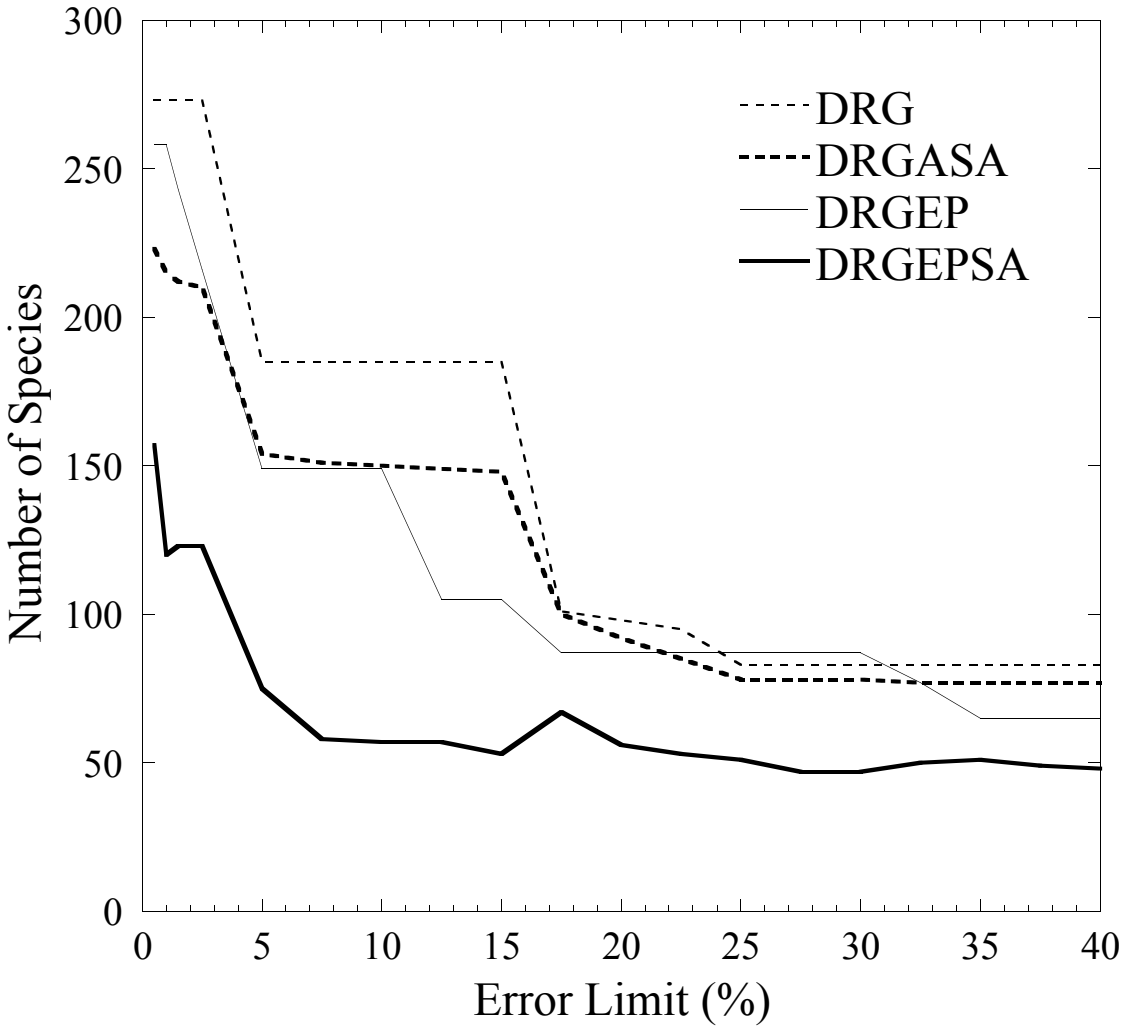

Figure 3.1: Number of species as a function of error limit for skeletal mechanisms for n-heptane generated using DRG, DRGEP, DRGASA, and DRGEPSA in the MARS implentation.

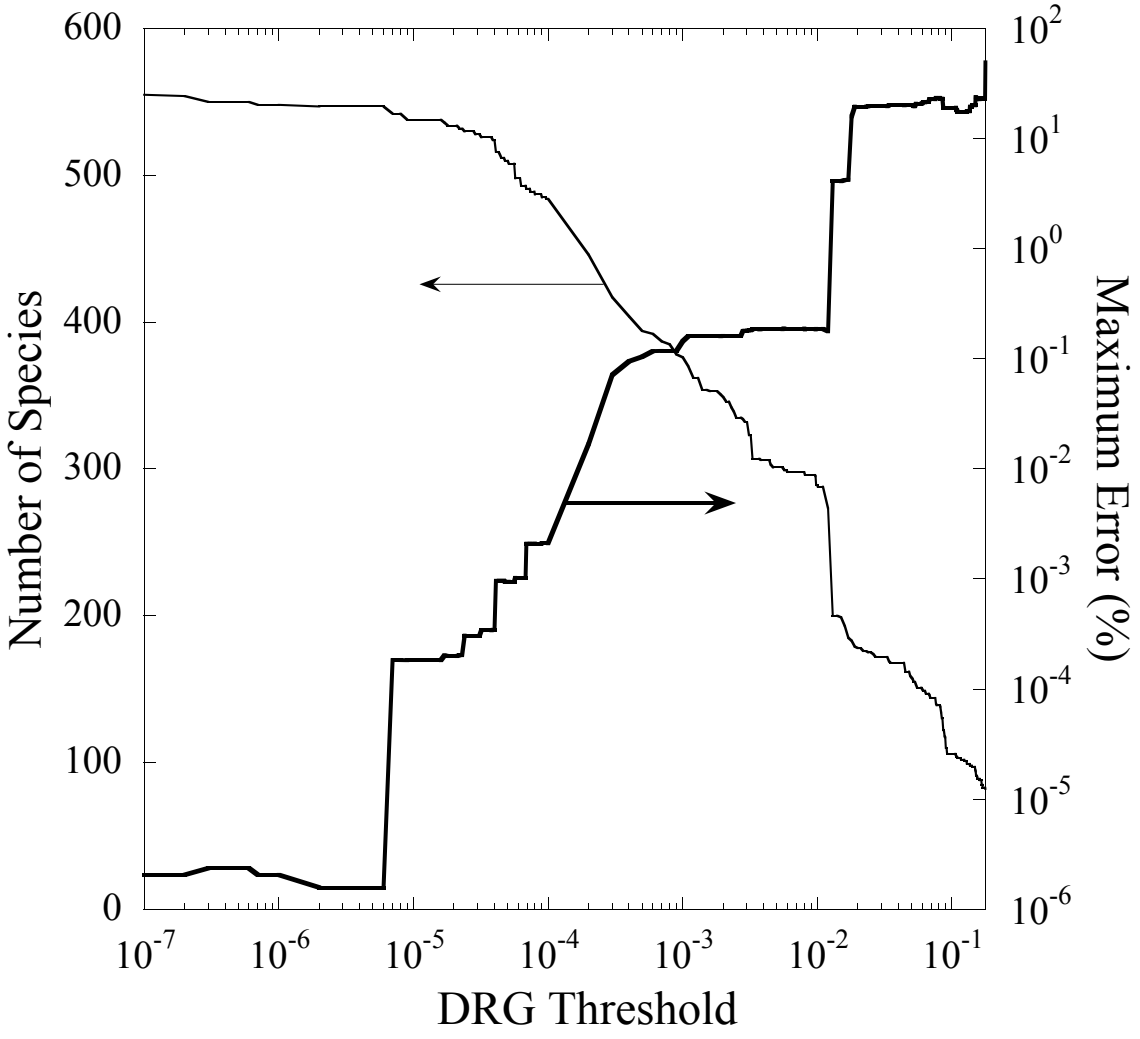

Figure 3.2: Number of species and maximum error of skeletal mechanisms for *n*-heptane generated by DRG using various threshold values (ε_{DRG}).

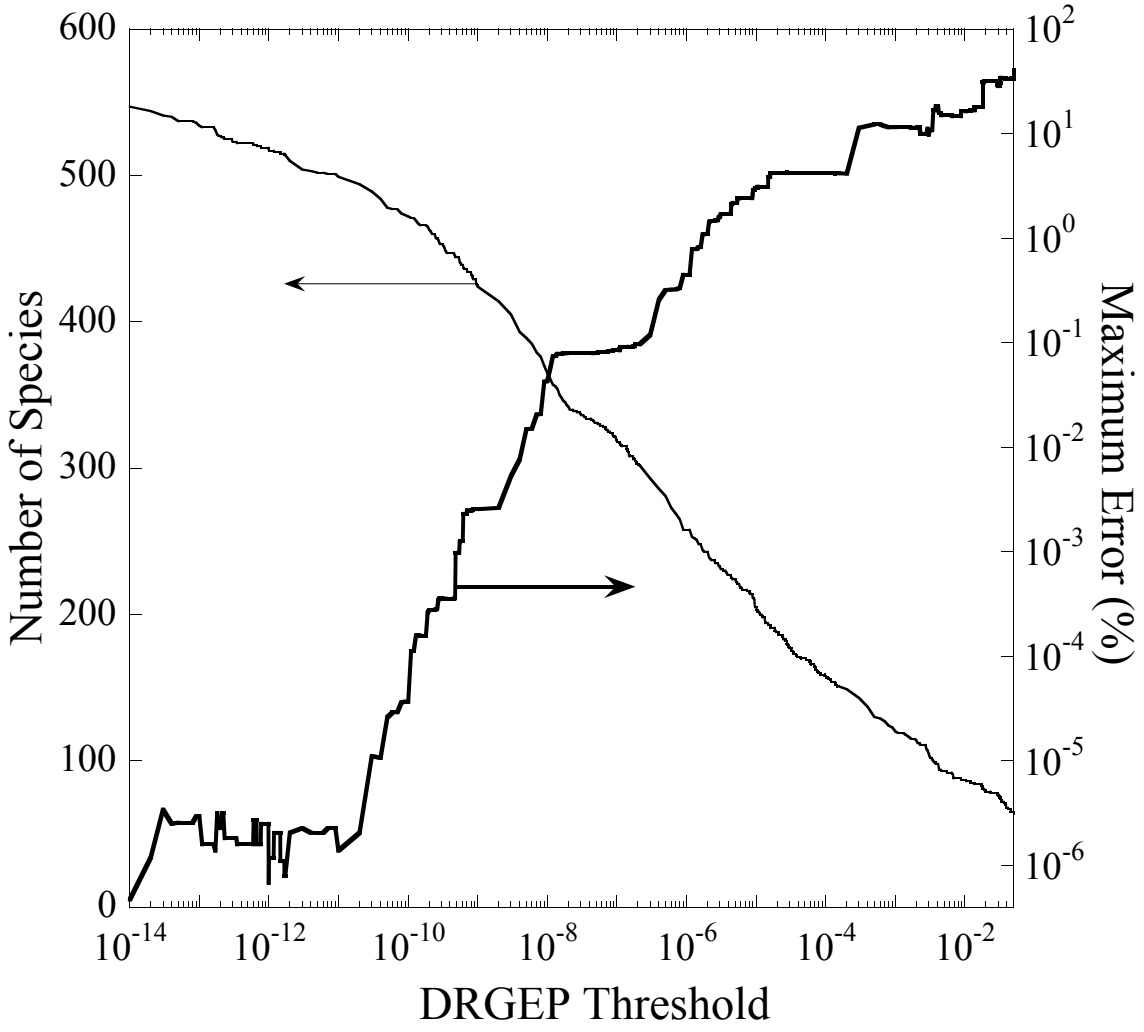

Figure 3.3: Number of species and maximum error of skeletal mechanisms for n-heptane generated by DRGEP using various threshold values (ε_{EP}).

expected, the number of species for skeletal mechanisms produced with both methods monotonically decreases with increasing error threshold. The relationship between the maximum error and error threshold is less clear, however. Additionally, the DRG method experiences large jumps in species number and maximum error, which coupled with the iterative threshold selection approach of MARS can explain similar jumps in species number for DRG and DRGASA seen in Fig. 3.1. DRGEP also experiences similar jumps, though smaller in size. This implies that the error threshold could be increased to produce slightly smaller skeletal mechanisms than those shown, though only to a certain extent as is demonstrated in Section 3.1.2.

3.1.2 Comprehensive *n*-Heptane Skeletal Reduction

Four skeletal mechanisms were generated using DRG, DRGASA, DRGEP, and DRGEPSA to illustrate the individual weaknesses of the DRGASA and DRGEP methods and the subsequent improvement of the combined method. The ignition delay error limit was 30% for the iterative error threshold selection as well as the sensitivity analysis phases of DRGASA and DRGEPSA. Autoignition chemical kinetics data were sampled from comprehensive initial conditions covering 600–1600 K, 1–20 atm, and equivalence ratios of 0.5–1.5.

The skeletal mechanism results for *n*-heptane are shown in Table 3.1. Through the iterative threshold selection procedure, 0.16 was selected as the optimal ε_{DRG} to generate a mechanism of 211 species using DRG while 0.01 was selected as the optimal ε_{EP} to generate a mechanism of 173 species using DRGEP. It is seen from Table 3.1 that the DRGEP and DRGASA methods generate mechanisms of comparable size while DRGEPSA produces a smaller skeletal mechanism for the same given error limit; all methods produce mechanisms of comparable performance. The mechanism sizes from the various methods are consistent with the earlier trends displayed in Section 3.1.1, though the inclusion of a larger range of initial conditions caused larger

Method	# Species	# Reactions	Max. Error
DRG	211	1044	21%
DRGASA	153	691	24%
DRGEP	173	868	28%
DRGEPSA	108	406	27%

Table 3.1: Comparison of n-heptane skeletal mechanism sizes generated by DRG, DRGEP, DRGASA, and DRGEPSA methods.

mechanisms sizes for the same error limit. The species in the skeletal mechanism generated by DRGEPSA are listed in Appendix A.

Validation of the DRGEP, DRGASA, and DRGEPSA skeletal mechanisms was performed and is shown in Fig. 3.4, covering initial conditions with temperatures of 600–1600 K, pressures of 1, 5, and 40 atm, and equivalence ratios of 0.5, 1.0, and 1.5. All three skeletal mechanisms exhibit good performance over the full range of conditions, but noticeable discrepancy (limited to 30% by the reduction procedure) occurs mainly in the negative temperature coefficient (NTC) region. It is interesting to note that at higher pressures, the larger DRGEP mechanism shows poorer performance in the NTC region than the smaller DRGASA and DRGEPSA mechanisms.

Figure 3.5 shows the induced errors compared to the OIC values of the species analyzed by sensitivity analysis (limbo species) in the DRGEPSA procedure. A highly nonlinear relationship is seen, illustrating the need for sensitivity analysis to further reduce the mechanism size. That is, simply increasing the ε_{EP} value would not be sufficient to remove unimportant species in this range of OIC values such that sensitivity analysis is needed following the DRGEP phase to generate a minimal skeletal mechanism. The OIC well identifies unimportant species but may lose accuracy for species of higher importance and induced error.

The improvement of DRGEPSA over DRGASA is evident by the smaller final skeletal mechanism with equivalent performance; DRGASA performs slightly better than DRGEP here, but the method cannot identify all unimportant species due to

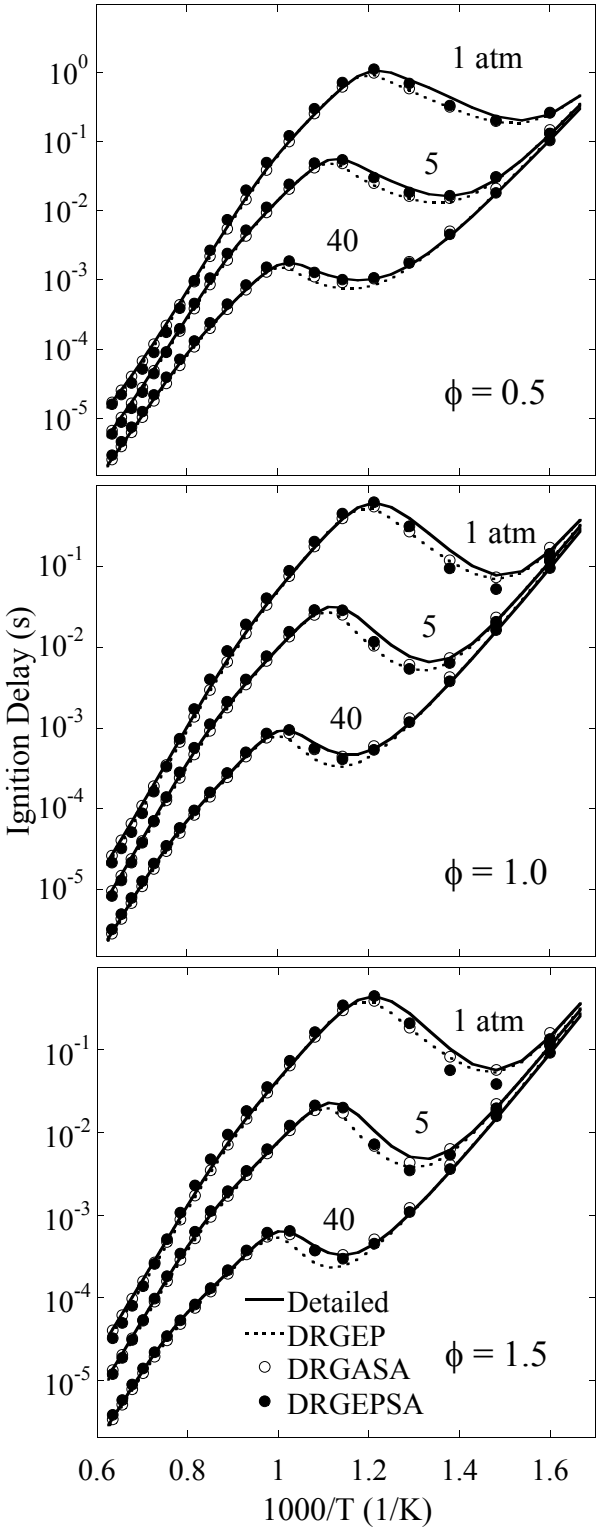

Figure 3.4: Autoignition validation of *n*-heptane skeletal mechanisms over a range of initial temperatures and pressures, and at varying equivalence ratios.

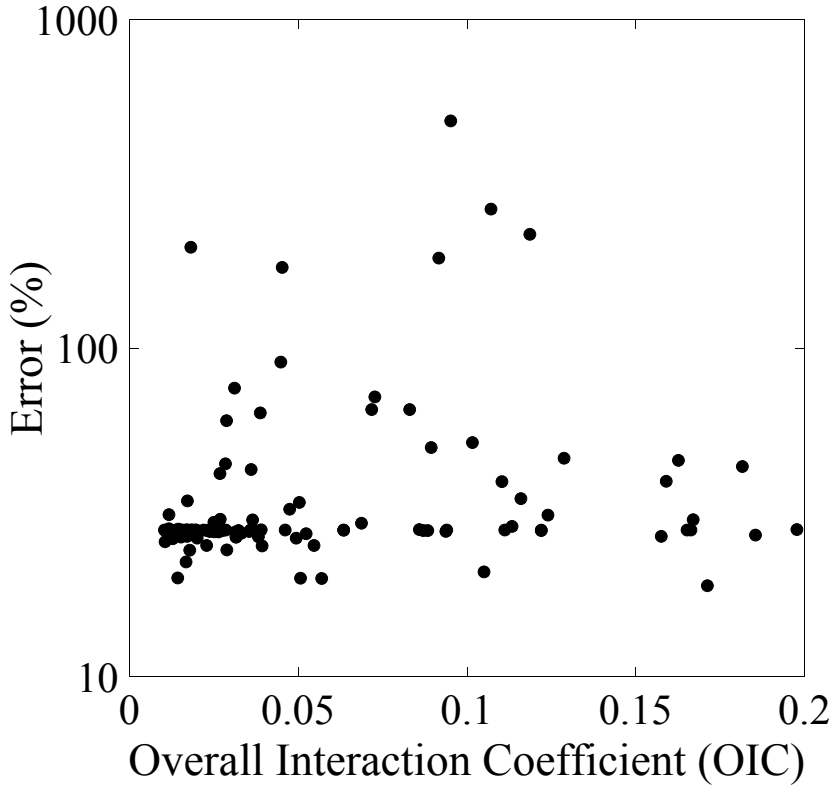

Figure 3.5: Induced error in ignition delay versus OIC values for species considered with sensitivity analysis phase in DRGEPSA during the n-heptane reduction.

Method	# Retained	# Limbo	# Removed
DRGASA	129	82	58
DRGEPSA	54	119	65

Table 3.2: Comparison of sensitivity analysis results using DRGASA and DRGEPSA methods.

species "shielding." This occurs because the DRG phase of DRGASA uses a DIC to rank species [54, 58, 62], which does not consider distance from targets and can inflate species importance such that species are automatically retained rather than assessed with sensitivity analysis. Table 3.2 contains the results of the sensitivity analysis phase from DRGASA and DRGEPSA in the current comparison. 46 species out of the 129 species automatically retained by DRGASA were eliminated from the final mechanism by DRGEPSA; specifically, 17 were removed by the DRGEP phase and 29 were removed by the SA phase in DRGEPSA, illustrating the shielding effect in DRGASA. Although eliminating the shielding increases the extent of total reduction, the greater number of species considered for sensitivity analysis can cause the DRGEPSA reduction to be more computationally expensive.

A skeletal mechanism for n-heptane was previously generated with a different implementation of the DRGASA method by Lu and Law [62, 64] using a two-stage DRG followed by sensitivity analysis. This approach used a similar autoignition initial condition range but also included perfectly-stirred reactor (PSR) kinetics data in the reduction procedure. The first stage of DRG, using $\varepsilon_{DRG} = 0.1$, produced an initial mechanism with 290 species, and the second stage, applying DRG again to the resulting mechanism, used $\varepsilon_{DRG} = 0.19$ to produce a skeletal mechanism with 188 species and 939 reactions. Following the sensitivity analysis phase, a final skeletal mechanism with 78 species and 359 reactions was obtained with approximately 30% maximum error. While this reduction provided a skeletal mechanism smaller than both the DRGASA and DRGEPSA mechanisms shown here, the purpose of the

current work is to compare the DRGEP, DRGASA, and DRGEPSA methods alone rather than specific strategies or implementations of employing such methods. The methods compared here used the same kinetics data and reduction procedure and differed only in the manner of ranking and selecting species for removal.

3.2 *iso*-Octane

iso-Octane is the other important PRF for gasoline with 100 on the octane scale [7, 76]. Four skeletal mechanisms from the detailed mechanism for *iso*-octane of Curran et al. [76], containing 857 species and 3606 reactions, were generated using DRG, DRGASA, DRGEP, and DRGEPSA to illustrate the greater reduction capability of the final method. All methods used the same constant volume autoignition data sampled from initial conditions ranging over 600–1600 K, 1–20 atm, and equivalence ratios of 0.5–1.5. The maximum error limit was 30%. Oxygen, nitrogen, *iso*-octane, and the hydrogen radical were selected as target species for all methods.

The skeletal reduction results for *iso*-octane are shown in Table 3.3. Through the iterative selection procedure, 0.15 was selected as the optimal ε_{DRG} and 0.004 as the optimal ε_{EP}. The results for the various mechanism sizes are consistent with the trends displayed in the *n*-heptane reductions; DRGEP and DRGASA produced mechanisms of comparable size and performance while DRGEPSA gives a mechanism substantially smaller than both for similar error. The species in the skeletal mechanism generated by DRGEPSA are listed in Appendix B.

Validation of the DRGASA and DRGEPSA skeletal mechanisms was performed and is shown in Fig. 3.6, covering temperatures of 600–1600 K, pressures of 1, 5, and 40 atm, and equivalence ratios of 0.5, 1.0, and 1.5. Good agreement between the ignition delay predictions of the skeletal mechanisms and the detailed mechanism is observed, with some discrepancy in the NTC region as in the *n*-heptane cases.

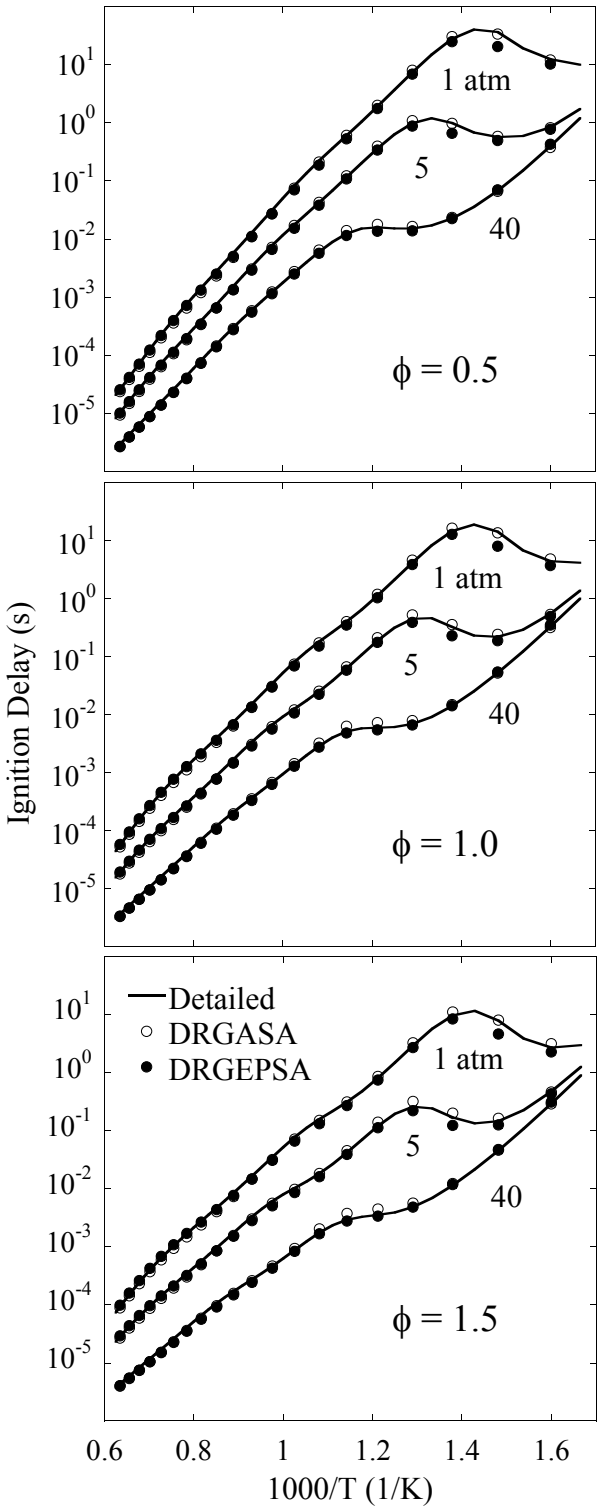

Figure 3.6: Autoignition validation of *iso*-octane skeletal mechanisms over a range of initial temperatures and pressures, and at varying equivalence ratios.

Method	# Species	# Reactions	Max. Error
DRG	275	722	13%
DRGASA	211	885	26%
DRGEP	232	1140	15%
DRGEPSA	165	779	19%

Table 3.3: Comparison of *iso*-octane skeletal mechanism sizes generated by DRG, DRGEP, DRGASA, and DRGEPSA methods.

Pepiot-Desjardins and Pitsch [65] generated skeletal mechanisms for *iso*-octane at various levels of complexity using an implementation of the DRGEP method. Autoignition chemical kinetics data covering a similar range of conditions to the current study were used, while the targets used were *iso*-octane, CO, CO_2, and temperature through heat release data. The relevant skeletal mechanism generated using DRGEP consisted of 196 species and 1762 irreversible reactions with a maximum error of 15%; this is of the same order as the DRGEP mechanism produced in the current study, though slightly smaller. In addition to a smaller error limit, their DRGEP implementation contains certain extensions not included in the current DRGEP, such as group-based DIC, scaling of DIC based on element flux, and an integrity check.

Similar to the strategy previously adopted for *n*-heptane, Xin et al. [77] recently presented a skeletal mechanism for *iso*-octane generated with the DRGASA method using a two-stage DRG phase. The reduction used a similar autoignition initial condition range to that of the current study, but included PSR in addition to autoignition chemical kinetics data. The first stage of DRG used $\varepsilon_{DRG} = 0.1$ to generate an initial mechanism with 347 species and the second stage used $\varepsilon_{DRG} = 0.17$ to generate a mechanism with 233 species and 959 reactions. After the sensitivity analysis phase, the final skeletal mechanism consisted of 112 species and 481 reactions. As in the *n*-heptane case, the two-stage DRG strategy in conjunction with DRGASA implementation is not being compared in the current work, only the DRGASA and DRGEPSA methods alone.

3.3 *n*-Decane

n-Decane is an important diesel surrogate component [9] and a primary component for jet fuel surrogates [11, 12]. Two skeletal mechanisms for *n*-decane were generated using the DRGEPSA method from the detailed mechanism for *n*-alkanes covering *n*-octane through *n*-hexadecane of Westbrook et al. [13] which contains 2115 species and 8157 reactions. The first skeletal reduction was performed using constant volume autoignition data sampled from initial conditions covering 600–1600 K and 1–20 atm, while the second skeletal reduction was limited to high-temperatures (1000–1300 K) and atmospheric pressure; both covered equivalence ratios of 0.5–1.5. The error limit for both reductions was 30%; oxygen, nitrogen, and *n*-decane were selected as target species for both reductions. In this case, selecting the hydrogen radical as an additional target did not increase the extent of reduction for the given error limit.

The DRGEP phase of the comprehensive reduction generated an initial skeletal mechanism with 381 species and 1865 reactions with a maximum error of 27% using $\varepsilon_{EP} = 1.4 \times 10^{-3}$ while the high-temperature reduction used $\varepsilon_{EP} = 0.007$ to generate a mechanism with 68 species and 391 reactions with a maximum error of 24%. The final comprehensive skeletal mechanism following sensitivity analysis consists of 202 species and 846 reactions with a maximum error of 25% and the high-temperature skeletal mechanism consists of 51 species and 256 reactions with a maximum error of 27%. The results are summarized in Table 3.4 for convenience. The species in the comprehensive and high-temperature skeletal mechanisms are listed in Appendices C and D, respectively.

Validation was performed using constant volume autoignition for both the comprehensive and high-temperature skeletal mechanisms covering pressures of 1, 5, and 40 atm and equivalence ratios of 0.5–1.5, with temperature ranges of 600–1600 K and 1000–1600 K shown in Figs. 3.7 and 3.8 respectively. The comprehensive mechanism well predicts the ignition delay compared to the detailed mechanism for the

Phase	# Species	# Reactions	Max. Error
	Comprehensive		
DRGEP	381	1865	27%
DRGEPSA	202	846	25%
	High-temperature		
DRGEP	68	391	24%
DRGEPSA	51	256	27%

Table 3.4: Summary of n-decane skeletal mechanism results.

full range of validation conditions, with some discrepancy in the NTC region. The high-temperature mechanism also shows fairly good performance, with noticeable discrepancies primarily in the low-temperature, high-pressure regions as expected.

Both skeletal mechanisms were also validated independently using PSR [78] and laminar flame speed simulations through PREMIX [79], phenomena not employed to generate kinetics data in the reduction procedure. Figures 3.9 and 3.10 show the validation of the comprehensive and high-temperature mechanisms in PSR with an inlet temperature of 300 K over pressures of 1, 5, and 40 atm, equivalence ratios of 0.5–1.5, and a range of residence times. The comprehensive mechanism well reproduces the curves and extinction turning points, with minor discrepancies only in the rich cases. The high-temperature mechanism also performs well here, with some discrepancies near the extinction turning points. Figures 3.11 and 3.12 show the validation in laminar flame speed calculations with an unburned mixture temperature of 400 K and pressures of 1, 5, and 40 atm over a range of equivalence ratios. The comprehensive skeletal mechanism performs quite well for all cases, with a maximum error of 12.3% at 5 atm, $\phi = 1.3$. The high-temperature mechanism also performs well here, with slight discrepancies in laminar flame speed predictions at all equivalence ratios at atmospheric pressure and larger error for the higher pressure cases at rich conditions.

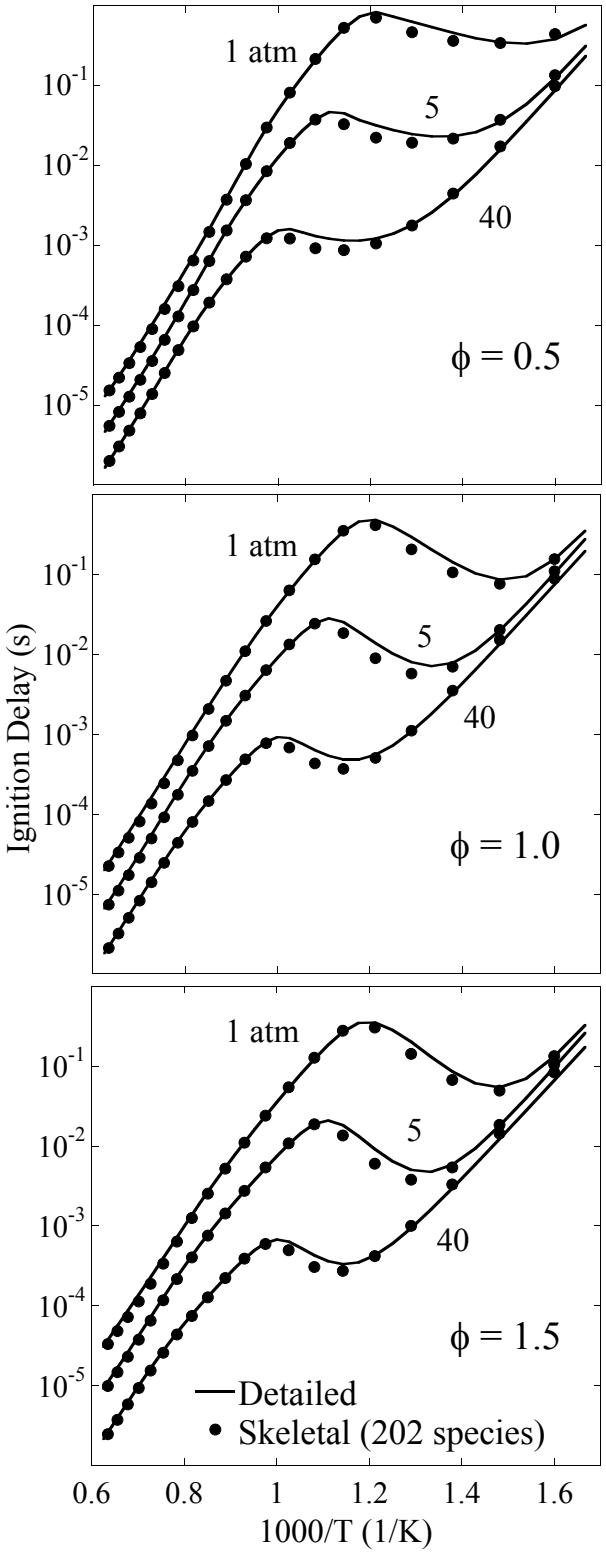

Figure 3.7: Autoignition validation of comprehensive n-decane skeletal mechanism (202 species and 846 reactions) over a range of initial temperatures and pressures, and at varying equivalence ratios.

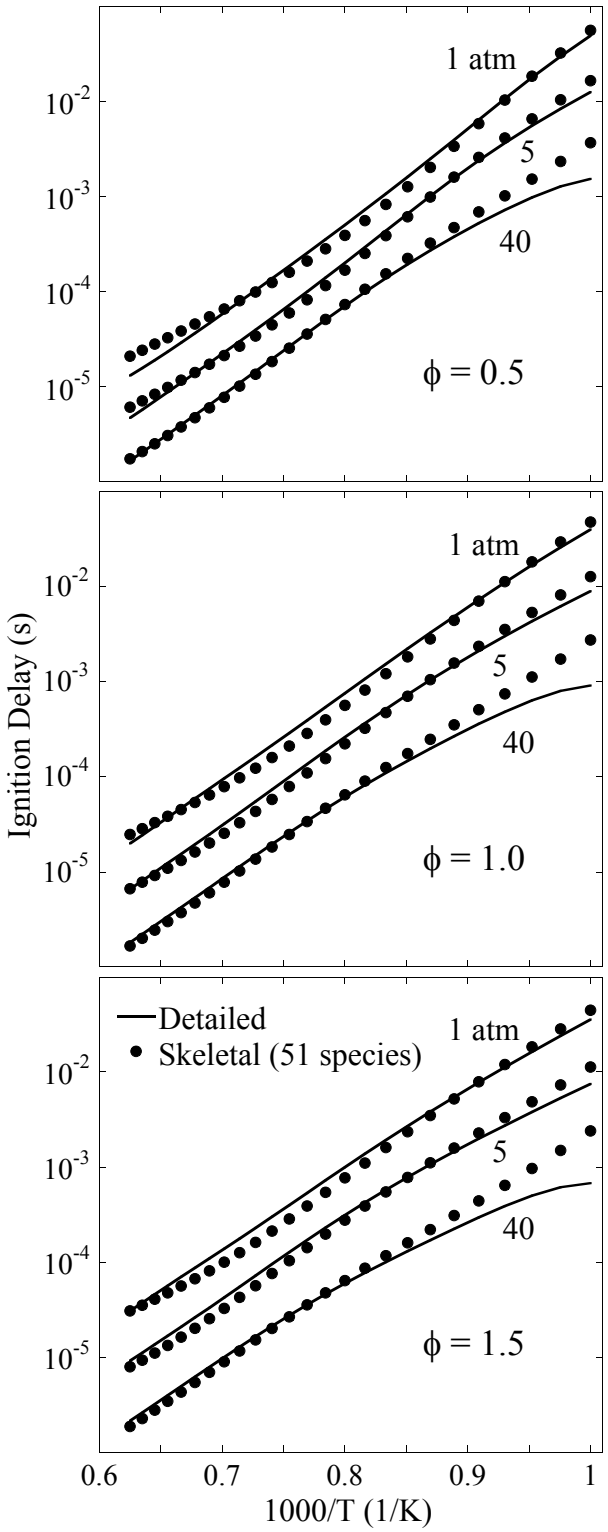

Figure 3.8: Autoignition validation of n-decane high-temperature skeletal mechanism over a range of initial temperatures and pressures, and at varying equivalence ratios.

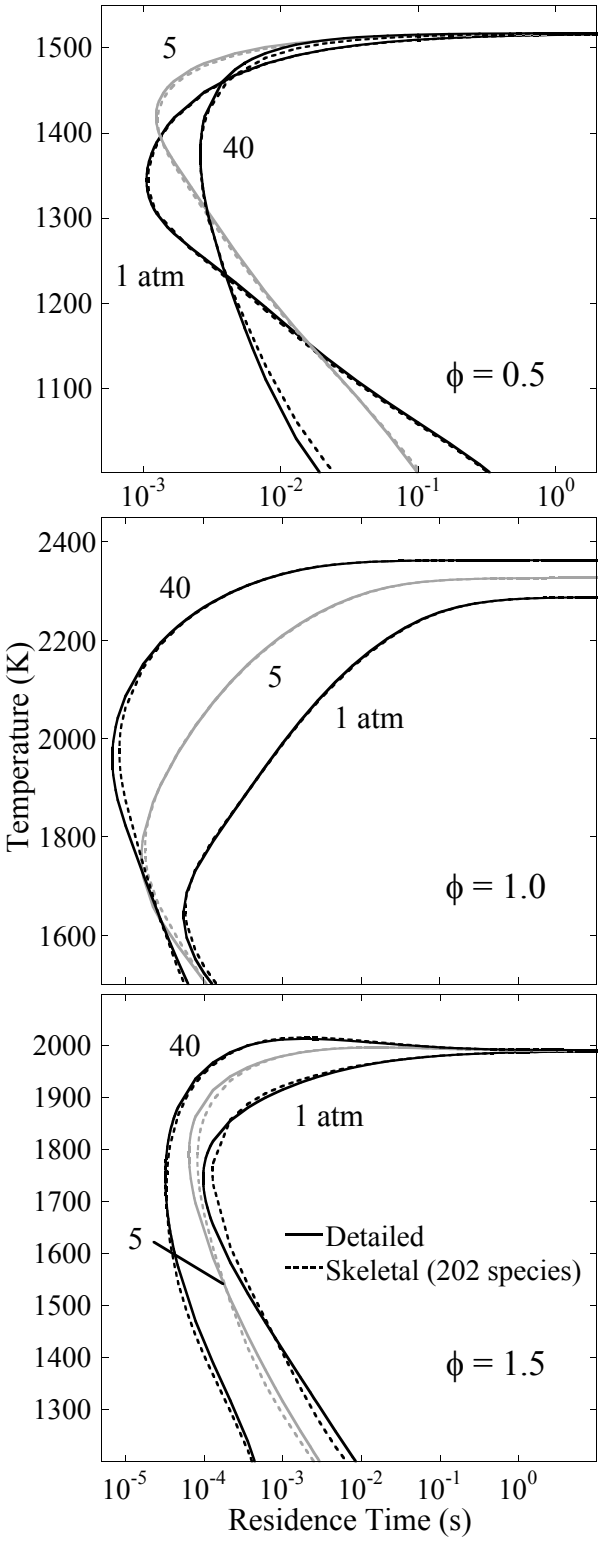

Figure 3.9: PSR validation of comprehensive n-decane skeletal mechanism (202 species and 846 reactions) over a range of residence times and at varying pressures and equivalence ratios with an inlet temperature of 300 K.

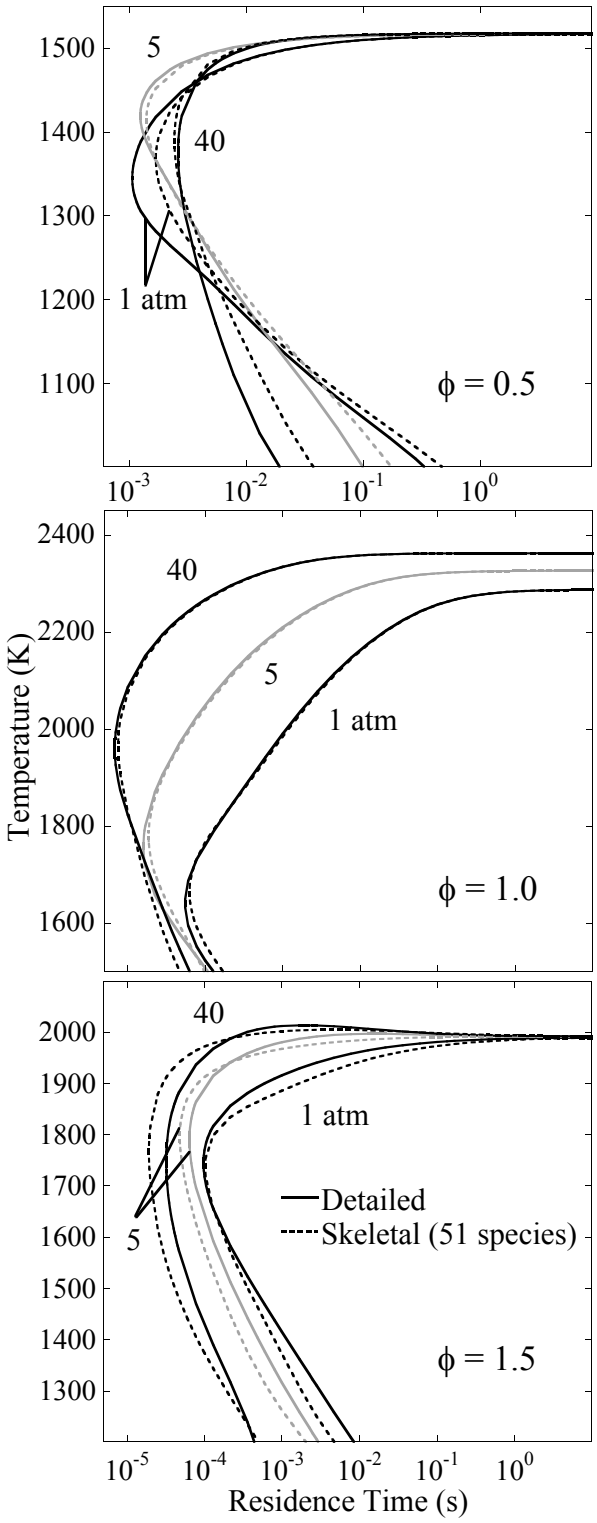

Figure 3.10: PSR validation of n-decane high-temperature skeletal mechanism over a range of residence times and at varying pressures and equivalence ratios with an inlet temperature of 300 K.

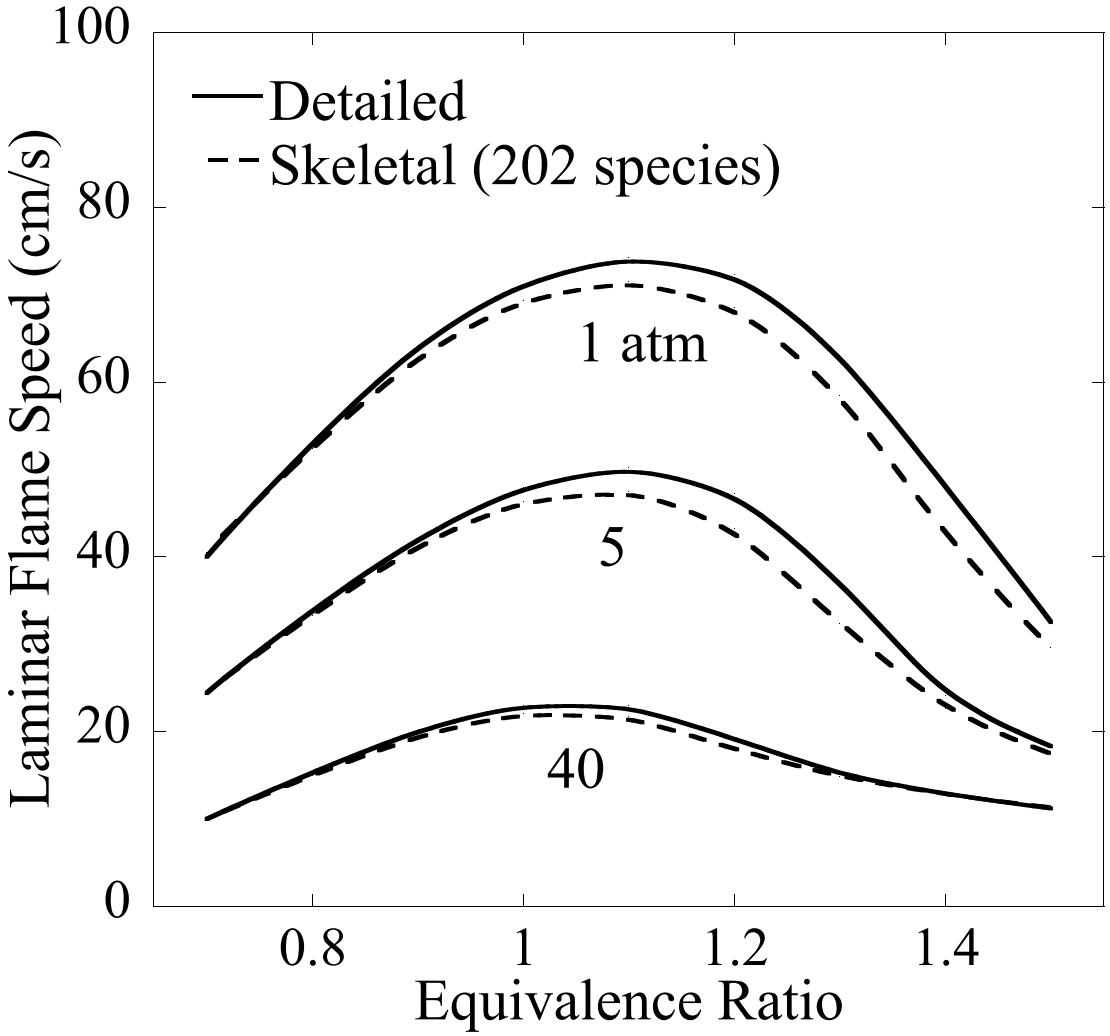

Figure 3.11: Laminar flame speed validation of comprehensive n-decane skeletal mechanism (202 species and 846 reactions) over a range of equivalence ratio and pressure conditions with an unburned mixture temperature of 400 K.

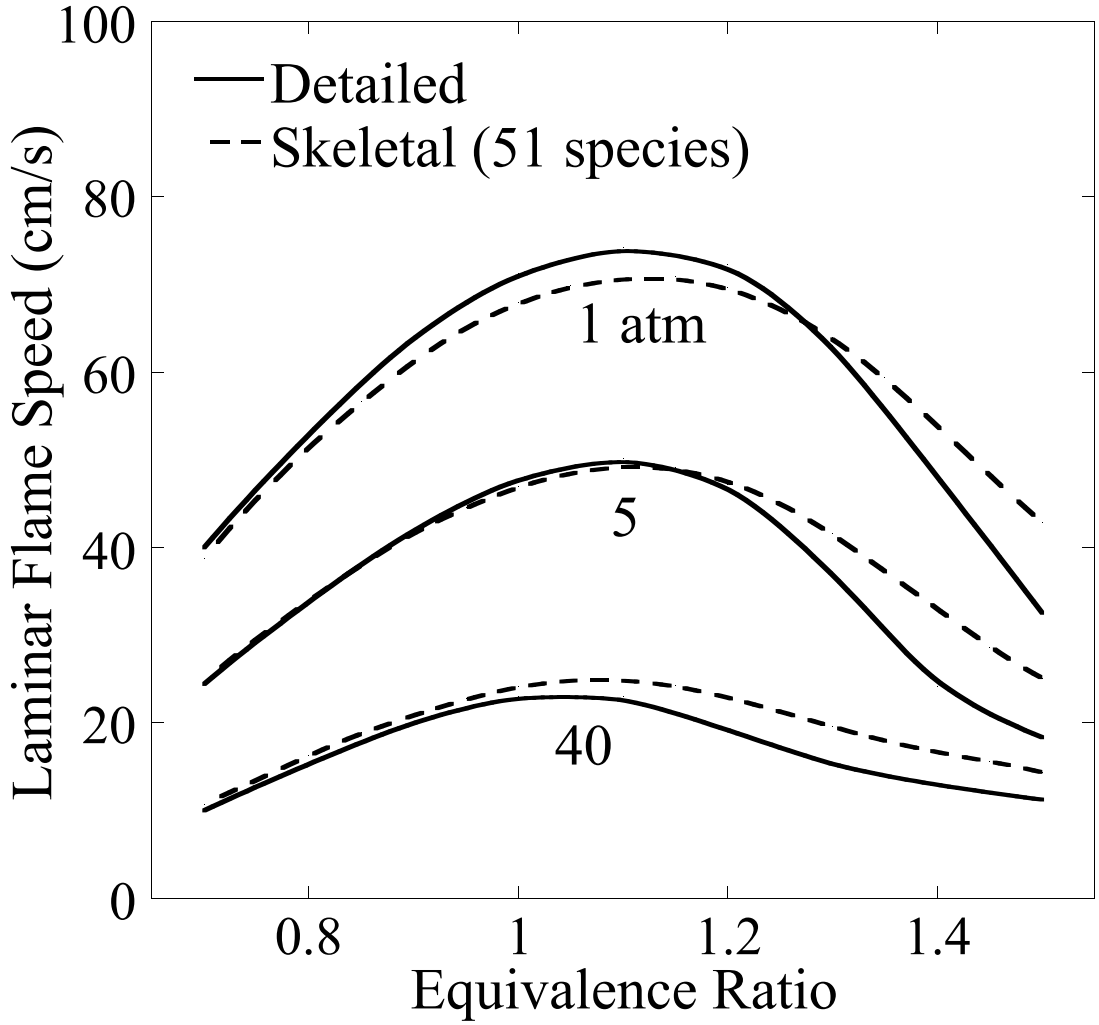

Figure 3.12: Laminar flame speed validation of n-decane high-temperature skeletal mechanism over a range of equivalence ratio and pressure conditions with an unburned mixture temperature of 400 K.

3.4 Discussion

In closing this chapter, the key findings of the previous sections are briefly summarized below. Here, I used the large detailed reaction mechanisms of three important surrogate components, *n*-heptane, *iso*-octane, and *n*-decane, to demonstrate the capability and adequacy of the overall reduction approach for the DRGEPA portion of MARS. The DRG, DRGEP, and DRGASA methods were also used to generate skeletal mechanisms for *n*-heptane and *iso*-octane for comparison, and for all the conditions considered DRGEPSA produced skeletal mechanisms of noticeably smaller sizes for equivalent performance. As shown in Section 3.1.1, DRGEPSA produced significantly smaller skeletal mechanisms even at more strict error limits. Additionally, the good external validation of the *n*-decane skeletal mechanisms validated the rationale that using constant volume autoignition simulations for chemical kinetics data sampling and error evaluation for the reduction procedure would produce valid skeletal mechanisms.

Chapter 4

Conclusions and Future Work

In the present work the Mechanism Automatic Reduction Software (MARS) implementation was presented and discussed, with an emphasis on the directed relation graph (DRG) with error propagation and sensitivity analysis (DRGEPSA) method for skeletal mechanism reduction. This approach, a combination of the DRG with error propagation (DRGEP) and DRG-aided sensitivity analysis (DRGASA) methods, utilizes the specific strengths of each individual method to diminish some of the weaknesses of each. DRGEP efficiently identifies and removes unimportant species while DRGASA incorporates sensitivity analysis to identify further unimportant species for removal at a greater computational expense. By combining the two methods, DRGEPSA is able to identify and remove more unimportant species than its precursors; however, the greater extent of reduction comes at a greater computational cost. Skeletal mechanisms of *n*-heptane were generated to illustrate the improvement of DRGEPSA over DRGEP and DRGASA, resulting in a final mechanism with 108 species compared to 173 and 153 species, respectively. Skeletal mechanisms of *iso*-octane were also presented to further illustrate the improvement of DRGEPSA over DRGEP and DRGASA, with final skeletal mechanisms of 165, 232, and 211 species, respectively. All skeletal mechanisms exhibit good ignition delay prediction compared

to the detailed mechanisms, with the most noticeable discrepancies in the negative temperature coefficient (NTC) regions.

Two skeletal mechanisms for n-decane were generated using DRGEPSA from a large detailed mechanism for n-alkanes, covering n-octane through n-hexadecane. One skeletal mechanism covers a comprehensive set of temperature conditions at low to high pressure while the other mechanism is limited to high-temperature conditions, and both mechanisms covered lean to rich equivalence ratios. The resulting comprehensive skeletal mechanism consists of 202 species and 846 reactions while the high-temperature mechanism is much smaller with 51 species and 256 reactions. The large extent of reduction for both mechanisms illustrates the capability of the DRGEPSA method to reduce large mechanisms of surrogate fuels.

External validation of the n-decane skeletal mechanisms was performed using perfectly-stirred reactor (PSR) and laminar flame (PREMIX) simulations. The comprehensive skeletal mechanism reproduces the results of the detailed mechanism in PSR with larger errors at higher pressure and rich conditions. The high-temperature skeletal mechanism also performs well, with larger errors at the lean, atmospheric pressure and rich, 40 atm pressure conditions. The comprehensive skeletal mechanism also performs quite well in predicting laminar flame speed with noticeable error at rich, higher pressure conditions. By comparison, the high-temperature skeletal mechanism fares slightly less better. Though only ignition chemical kinetics data were used in the mechanism reduction procedure, both mechanisms perform well predicting the extinction turning point in PSR and even for predicting laminar flame speed where transport phenomena are considered. It is further noted that if a posteriori validation is not satisfactory, the range of overall interaction coefficient values used to identify limbo species could be adjusted. Alternatively, PSR and/or PREMIX simulations could be included in the chemical kinetics data sampling and for error evaluation.

While a significant reduction is achieved with the comprehensive skeletal mechanisms (approximately 10% of the detailed mechanism for n-decane) using DRGEPSA, the final mechanisms are still too large to be used in full-scale three-dimensional simulations. The compact size of the high-temperature skeletal mechanism illustrates the significant reduction capability when the input conditions are limited to the desired range. For instance, flame simulations rely largely on high-temperature chemistry such that a skeletal mechanism desired for this purpose could omit the complex low-temperature and NTC regime chemistry with acceptable error. The current high-temperature skeletal mechanism with 51 species and 256 reactions could be used without further reduction in large-scale simulations.

Future work will be done to both investigate the DRGEPSA method and improve the MARS implementation. In particular, further investigation is needed on the species whose importance is not well captured by DRG/DRGEP coefficients, as mentioned in Section 3.1. If these species can be better identified prior to sensitivity analysis (SA), the computational expense of the entire DRGEPSA method could be reduced. This is also related to a smarter iterative threshold selection, as mentioned in Section 2.3, and an adaptive upper threshold selection, as discussed in Section 2.4, which could produce smaller final mechanisms as well as eliminate unnecessary SA.

Extensions to the current MARS program, as shown in Fig. 2.1 such as unimportant reaction elimination, isomer lumping, diffusive species bundling, and computational singular perturbation (CSP)-based quasi-steady state (QSS) reduction, will also be pursued. Nagy and Turányi [61] suggested that removal of additional unimportant reactions could significantly improve the computational cost of simulations. Additional skeletal reduction steps such as isomer lumping and diffusive species bundling, which have been investigated by Lu and Law [15, 64, 80], are required before realistic computational simulations are feasible with comprehensive skeletal mechanisms such as those presented here. Additionally, time-scale reduction will be pursued. Initial

work has been completed that uses CSP methodology to identify QSS species and successive algebraic iterations to solve for the QSS species concentrations. As discussed by Law et al. [4], however, such an approach can run into problems converging and even introduce greater computational cost than not applying the QSS approximation. Lu and Law [81] introduced an approach that both linearized the QSS relations and solved for the QSS concentrations analytically, but proposed that a hybrid iterative-analytic solution scheme would be necessary for larger reaction mechanisms. Such an approach will be investigated for the larger surrogate component mechanisms considered here.

Appendices:

Lists of Species in Skeletal Mechanisms Generated using DRGEPSA

Appendix A

n-Heptane Comprehensive Skeletal Mechanism

The symbols representing species follow the same naming convention as the detailed mechanism for *n*-heptane of Curran et al. [75, 76], available at:

https://www-pls.llnl.gov/?url=science_and_technology-chemistry-combustion-nc7h16

h	ch3o	c3h4-p	c2h5o2
h2	c2h6	c3h6	ch3o2h
o	c2h4	c4h6	c2h4o2h
o2	c2h5	nc3h7	o2c2h4oh
oh	c2h	ic3h7	c2h3co
h2o	c2h2	c4h7	c2h3cho
n2	c2h3	c4h8-1	c3h5o
co	ch2oh	pc4h9	nc3h7o
hco	ch2co	ch3coch2	c4h7o
co2	hcco	c2h5cho	c4h8ooh1-3o2
ch3	pc2h4oh	c5h10-1	c4h8ooh1-3
ch4	ch3co	c5h11-1	c4h8o1-3
ho2	ch2cho	c5h11-2	pc4h9o2
h2o2	ch3cho	c2h5o	c5h11o2-1
ch2o	c3h4-a	ch3o2	c5h10ooh1-3

c5h10ooh1-3o2	hoch2o	c7h15o2-2	c7h14ooh4-2o2
ch2(s)	hocho	c7h15o2-3	c7h14o1-2
nc4ket13	c6h13-1	c7h15o2-4	c7h14o1-3
nc5ket13	c6h12-1	c7h14ooh1-3	c7h14o1-4
nc3h7cho	c6h11	c7h14ooh2-4	c7h14o2-3
c2h5coch2	nc7h16	c7h14ooh2-5	c7h14o2-4
ch3chcoch3	c7h15-1	c7h14ooh3-5	c7h14o2-5
ch3chco	c7h15-2	c7h14ooh3-6	c7h14o3-5
c2h5chco	c7h15-3	c7h14ooh4-2	nc7ket13
nc3h7coch2	c7h15-4	c7h14ooh1-3o2	nc7ket24
nc4h9cho	c7h14-1	c7h14ooh2-4o2	nc7ket35
nc4h9co	c7h15o2-1	c7h14ooh3-5o2	nc7ket42

Appendix B

iso-Octane Comprehensive Skeletal Mechanism

The symbols representing species follow the same naming convention as the detailed mechanism for *iso*-octane of Curran et al. [76], available at:

https://www-pls.llnl.gov/?url=science_and_technology-chemistry-combustion-ic8h18

h	ch3o	c3h6	c2h3co
h2	c2h6	ic3h7	c2h3cho
o	c2h4	ic4h7	c3h5o
o2	c2h5	ic4h8	c3h6ooh2-1
oh	c2h	tc4h9	ic3h7o
h2o	c2h2	ic4h9	ic3h7o2h
n2	c2h3	ic4h10	ic3h7o2
co	ch3oh	ch3coch3	ic4h8o
hco	ch2oh	ch3coch2	ic4h8oh
co2	ch2co	c2h5co	io2c4h8oh
ch3	hcco	ac5h10	ic4h7o
ch4	ch3co	neoc5h11	ic4h8ooh-io2
ho2	ch3cho	ch3o2	ic4h8o2h-i
h2o2	c3h4-a	ch3o2h	ic4h8o2h-t
ch2o	c3h4-p	ch3co2	tc4h8o2h-i

ic4h9o
tc4h9o
ic4h9o2h
tc4h9o2h
tc4h9o2
ic4h9o2
ch3coch2o2
ch3coch2o2h
ch3coch2o
neoc5ketox
neoc5h11o2
neoc5h11o
neoc5h10ooh
neoc5h10ooh-o2
c3h5-a
c3h5-s
c3h5-t
c3h3
c3h2
ho2cho
o2cho
ch2(s)
ic4ketii
neoc5ket
ic4h7ooh
ic3h5cho
tc3h6cho
ic3h7cho
ic3h6co
ic4h6oh
ic3h5co
ic3h7co
tc3h6o2cho
tc3h6o2hco
ch2cch2oh
ch3chcoch3
ch3chco
ch3chcho
c2h3chcho
neoc5h9q2-n
hoch2o
hocho
ic6h11
tc4h9cho
tc4h9co
neoc5h11co
c4h7cho2-2
xc7h15
yc7h15
xc7h14
yc7h14
xc7h13
yc7h15o2
pc7h15
oc7h14
p-qc7h14o
ic8h18
ac8h17
bc8h17
cc8h17
dc8h17
ic8h15
ac8h17o2
bc8h17o2
cc8h17o2
dc8h17o2
ac8h17o2h
bc8h17o2h
cc8h17o2h
dc8h17o2h
ac8h17o
bc8h17o
cc8h17o
dc8h17o
ac8h16ooh-b
ac8h16ooh-c
bc8h16ooh-c
bc8h16ooh-a
bc8h16ooh-d
cc8h16ooh-a
dc8h16ooh-b
ic8eteraa
ic8eterab
ic8eterac
ic8eterbc
ic8eterbd
ic8eterdd
ac8h16ooh-bo2
bc8h16ooh-co2
bc8h16ooh-ao2
bc8h16ooh-do2
dc8h16ooh-bo2
ic8ketab
ic8ketba
ic8ketbc
ic8ketbd
ic8ketdb
ic3h7coc3h6-t
tc4h9coc2h4s
yc7h13ooh-x1
yc7h13o-x1
xc7h13o-z
yc7h13ooh-x2
yc7h13o-x2
cc6h11o-b

Appendix C

n-Decane Comprehensive Skeletal Mechanism

The symbols representing species follow the same naming convention as the detailed mechanism for n-alkanes C_8 – C_{16} of Westbrook et al. [13], available at:

www-pls.llnl.gov/?url=science_and_technology-chemistry-combustion-c8c16_n_alkanes

h	ch3o	ch3cho	c5h10-2
h2	c2h6	c3h4-a	bc5h10
o	c2h4	c3h4-p	cc5h10
o2	c2h5	c3h6	c5h11-1
oh	ch2	c4h6	c5h11-2
h2o	c2h	nc3h7	c2h5o
n2	c2h2	ic4h7	ch3o2
co	c2h3	c4h7	c2h5o2
hco	ch3oh	c4h8-2	ch3o2h
co2	ch2oh	c4h8-1	c2h4o1-2
ch3	ch2co	pc4h9	c2h4o2h
ch4	hcco	ch3coch2	o2c2h4oh
ho2	pc2h4oh	c2h5cho	c2h3co
h2o2	ch3co	c5h9	c2h3cho
ch2o	ch2cho	c5h10-1	c3h5o

c3h6ooh1-2
nc3h7o
nc3h7o2
c4h7o
c4h8oh-1
c4h8oh-1o2
c4h8ooh1-3o2
c4h8ooh1-2
c4h8ooh1-3
c4h8ooh1-4
c4h8o1-3
c4h8o1-4
pc4h9o
pc4h9o2
c5h11o2-1
c5h10ooh1-3
c5h10ooh1-4
c5h10ooh1-3o2
c5h10o1-4
c3h5-a
c3h5-t
c3h6o1-2
ch2(s)
nc4ket13
nc5ket13
nc3h7cho
nc3h7co
c2h5coch2
ch3chcoch3
ch3chco
ch2ch2cho
c3h6cho-1
nc3h7coch2
nc4h9cho
nc4h9co
hoch2o
hocho
c6h13-1
c6h13-2
c6h12-1
c6h11
c6h12o1-4
c6h13o2-1
c6h12ooh1-3
c6h12ooh1-4
c6h12ooh1-3o2
nc6ket13
c7h15-1
c7h15-4
c7h14-1
c7h13
c7h15o2-1
c7h14ooh1-3
c7h14ooh1-4
c7h14ooh1-3o2
c7h14o1-3
c7h14o1-4
nc7ket13
nc5h11cho
nc5h11co
nc4h9coch2
c4h7ooh1-4
c4h7o1-4
nc10h22
c10h21-1
c10h21-2
c10h21-3
c10h21-4
c10h21-5
c9h19-1
c8h17-1
c8h17-4
c10h20-2
c9h18-1
c8h16-1
c8h16-4
c10h21o-1
c10h21o-2
c10h21o-3
c10h21o-4
c10h21o-5
c10h21o2-1
c10h21o2-2
c10h21o2-3
c10h21o2-4
c10h21o2-5
c8h17o2-1
c10h21o2h-2
c10ooh1-3
c10ooh1-4
c10ooh2-3
c10ooh2-4
c10ooh2-5
c10ooh3-1
c10ooh3-5
c10ooh3-6
c10ooh4-2
c10ooh4-6
c10ooh4-7
c10ooh5-2
c10ooh5-3
c10ooh5-7
c10ooh5-8
c8ooh1-3
c8ooh1-4
c10ooh1-3o2
c10ooh2-3o2
c10ooh2-4o2
c10ooh3-1o2
c10ooh3-5o2
c10ooh4-2o2
c10ooh4-6o2
c10ooh5-3o2
c10ooh5-7o2
c8ooh1-3o2
c10o1-3
c10o1-4
c10o2-4
c10o2-5
c10o3-5
c10o3-6
c10o4-6
c10o4-7
c10ket1-3
c10ket2-3
c10ket2-4
c10ket3-1
c10ket3-5
c10ket4-2
c10ket4-6
c10ket5-3
c10ket5-7

c8ket1-3	nc7h15co	c6h13coch2	c8h15
nc7h15cho	nc6h13co	c5h11coch2	
nc6h13cho	c7h15coch2	c10h19	

Appendix D

n-Decane High-Temperature Skeletal Mechanism

The symbols representing species follow the same naming convention as the detailed mechanism for *n*-alkanes C_8 – C_{16} of Westbrook et al. [13], available at:

www-pls.llnl.gov/?url=science_and_technology-chemistry-combustion-c8c16_n_alkanes

h	h2o2	nc3h7	c6h12-1
h2	ch2o	c4h7	c6h11
o	ch3o	c4h8-1	c7h15-1
o2	c2h6	pc4h9	nc10h22
oh	c2h4	c5h10-1	c10h21-1
h2o	c2h5	c5h11-1	c10h21-2
n2	c2h2	c5h11-2	c10h21-3
co	c2h3	c2h5o	c10h21-4
hco	hcco	c2h3co	c10h21-5
co2	ch2cho	c2h3cho	c9h19-1
ch3	ch3cho	c3h5o	c8h17-1
ch4	c3h6	c3h5-a	c8h16-1
ho2	c4h6	c6h13-1	

Bibliography

[1] Basic Energy Sciences Workshop, Office of Science, U.S. Department of Energy. Basic research needs for clean and efficient combustion of 21st century transportation fuels, Apr. 2006.

[2] C. K. Law. Combustion at a crossroads: Status and prospects. *Proc. Combust. Inst.*, 31:1–29, 2007.

[3] C. K. Westbrook, Y. Mizobuchi, T. Poinsot, P. J. Smith, and J. Warnatz. Computational combustion. *Proc. Combust. Inst.*, 30:125–157, 2005.

[4] C. K. Law, C.-J. Sung, H. Wang, and T. Lu. Development of comprehensive detailed and reduced reaction mechanisms for combustion modeling. *AIAA J.*, 41(9):1629–1646, 2003.

[5] M. O. Conaire, H. Curran, J. Simmie, W. Pitz, and C. Westbrook. A comprehensive modeling study of hydrogen oxidation. *Int. J. Chem. Kinet.*, 36(11):603–622, 2004.

[6] G. P. Smith, D. M. Golden, M. Frenklach, N. W. Moriarty, B. Eiteneer, M. Goldenberg, C. T. Bowman, R. K. Hanson, S. Song, J. William C. Gardiner, V. V. Lissianski, and Z. Qin. GRI-Mech 3.0. http://www.me.berkeley.edu/gri_mech/.

[7] W. J. Pitz, N. P. Cernansky, F. Dryer, F. Egolfopoulos, J. T. Farrell, D. Friend,

and H. Pitsch. Development of an experimental database and chemical kinetic models for surrogate gasoline fuels. SAE 2007-01-0175, 2007.

[8] F. Battin-Leclerc. Detailed chemical kinetic models for the low-temperature combustion of hydrocarbons with application to gasoline and diesel fuel surrogates. *Prog. Energy Comb. Sci.*, 34(4):440–498, 2008.

[9] J. T. Farrell, N. P. Cernansky, F. Dryer, D. Friend, C. A. Hergart, C. K. Law, R. M. McDavid, C. J. Mueller, A. K. Patel, and H. Pitsch. Development of an experimental database and kinetic models for surrogate diesel fuels. SAE 2007-01-0201, 2007.

[10] A. Violi, S. Yan, E. Eddings, F. Sarofim, S. Granata, T. Faravelli, and E. Ranzi. Experimental formulation and kinetic model for JP-8 surrogate mixtures. *Combust. Sci. Technol.*, 174(11-2):399–417, 2002.

[11] M. Colket, T. Edwards, S. Williams, N. P. Cernansky, D. L. Miller, F. Egolfopoulos, P. Lindstedt, K. Seshadri, F. Dryer, C. K. Law, D. Friend, D. B. Lenhert, H. Pitsch, A. F. Sarofim, M. Smooke, and W. Tsang. Development of an experimental database and kinetic models for surrogate jet fuels. In *45th AIAA Aerospace Sciences Meeting*, number AIAA 2007-770, 2007.

[12] M. Colket, T. Edwards, S. Williams, N. P. Cernansky, D. L. Miller, F. Egolfopoulos, F. Dryer, J. Bellan, P. Lindstedt, K. Seshadri, H. Pitsch, A. Sarofim, M. Smooke, and W. Tsang. Identification of target validation data for development of surrogate jet fuels. In *46th AIAA Aerospace Sciences Meeting*, number AIAA 2008-972, 2008.

[13] C. K. Westbrook, W. J. Pitz, O. Herbinet, H. J. Curran, and E. J. Silke. A comprehensive detailed chemical kinetic reaction mechanism for combustion

of n-alkane hydrocarbons from n-octane to n-hexadecane. *Combust. Flame*, 156(1):181–199, 2009.

[14] O. Herbinet, W. J. Pitz, and C. K. Westbrook. Detailed chemical kinetic oxidation mechanism for a biodiesel surrogate. *Combust. Flame*, 154(3):507–528, 2008.

[15] T. Lu and C. K. Law. Toward accommodating realistic fuel chemistry in large-scale computations. *Prog. Energy Comb. Sci.*, 35(2):192–215, 2009.

[16] J. F. Griffiths. Reduced kinetic models and their application to practical combustion systems. *Prog. Energy Comb. Sci.*, 21(1):25–107, 1995.

[17] A. S. Tomlin, T. Turányi, and M. J. Pilling. *Mathematical tools for the construction, investigation and reduction of combustion mechanisms*, volume 35, chapter 4, pages 293–437. Elsevier, Amsterdam, 1997.

[18] M. S. Okino and M. Mavrovouniotis. Simplification of mathematical models of chemical reaction systems. *Chem. Rev.*, 98(2):391–408, 1998.

[19] M. Bodenstein. Eine theorie der photomechnischen reaktionsgeschwindigkeit. *Z. Phys. Chem.*, 85:329–397, 1913.

[20] D. Chapman and L. Underhill. The interaction of chlorine and hydrogen. The influence of mass. *J. Chem. Soc., Trans.*, 103:496–508, 1913.

[21] S. W. Benson. The induction period in chain reactions. *J. Chem. Phys.*, 20(10):1605–1612, 1952.

[22] J. D. Ramshaw. Partial equilibrium in fluid dynamics. *Phys. Fluids*, 23(4):675–680, 1980.

[23] J.-Y. Chen. A general procedure for constructing reduced reaction mechanisms with given independent relations. *Combust. Sci. Technol.*, 57(1-3):89–94, 1988.

[24] T. Lu, C. K. Law, C. S. Yoo, and J. H. Chen. Dynamic stiffness removal for direct numerical simulations. *Combust. Flame*, 156(8):1542–1551, 2009.

[25] U. Maas and S. B. Pope. Simplifying chemical kinetics: Intrinsic low-dimensional manifolds in composition space. *Combust. Flame*, 88(3-4):239–264, 1992.

[26] S. B. Pope. Computationally efficient implementation of combustion chemistry using in situ adaptive tabulation. *Combust. Theor. Model.*, 1(1):41–63, 1997.

[27] S.-H. Lam and D. A. Goussis. Understanding complex chemical kinetics with computational singular perturbation. *Proc. Combust. Inst.*, 22:931–941, 1988.

[28] S.-H. Lam. Using CSP to understand complex chemical kinetics. *Combust. Sci. Technol.*, 89(5-6):375–404, 1993.

[29] S.-H. Lam and D. A. Goussis. The CSP method for simplying kinetics. *Int. J. Chem. Kinet.*, 26(4):461–486, 1994.

[30] T. Lu, Y. Ju, and C. K. Law. Complex CSP for chemistry reduction and analysis. *Combust. Flame*, 126(1-2):1445–1455, 2001.

[31] T. Lu and C. K. Law. A criterion based on computational singular perturbation for the identification of quasi steady state species: A reduced mechanism for methane oxidation with NO chemistry. *Combust. Flame*, 154(4):761–774, 2008.

[32] G. Li and H. Rabitz. A general analysis of exact lumping in chemical kinetics. *Chem. Eng. Sci.*, 44(6):1413–1430, 1989.

[33] H. Huang, M. Fairweather, J. F. Griffiths, A. S. Tomlin, and R. B. Brad. A systematic lumping approach for the reduction of comprehensive kinetic models. *Proc. Combust. Inst.*, 30:1309–1316, 2005.

[34] P. Pepiot-Desjardins and H. Pitsch. An automatic chemical lumping method for the reduction of large chemical kinetic mechanisms. *Combust. Theor. Model.*, 12(6):1089–1108, 2008.

[35] K. Edwards, T. Edgar, and V. Manousiouthakis. Kinetic model reduction using genetic algorithms. *Comput. Chem. Eng.*, 22(1-2):239–246, 1998.

[36] L. Elliott, D. Ingham, A. Kyne, N. Mera, M. Pourkashanian, and C. Wilson. Genetic algorithms for optimisation of chemical kinetics reaction mechanisms. *Prog. Energy Comb. Sci.*, 30(3):297–328, 2004.

[37] B. Bhattacharjee, D. Schwer, P. I. Barton, and W. Green. Optimally-reduced kinetic models: reaction elimination in large-scale kinetic mechanisms. *Combust. Flame*, 135(3):191–208, 2003.

[38] O. O. Oluwole, B. Bhattacharjee, J. Tolsma, P. I. Barton, and W. Green. Rigorous valid ranges for optimally reduced kinetic models. *Combust. Flame*, 146(1-2):348–365, 2006.

[39] A. Mitsos, G. Oxberry, P. I. Barton, and W. Green. Optimal automatic reaction and species elimination in kinetic mechanisms. *Combust. Flame*, 155:118–132, 2008.

[40] T. Løvås, F. Mauss, C. Hasse, and N. Peters. Development of adaptive kinetics for application in combustion systems. *Proc. Combust. Inst.*, 29(1):1403–1410, 2002.

[41] D. Schwer, P. Lu, and W. Green. An adaptive chemistry approach to modeling complex kinetics in reacting flows. *Combust. Flame*, 133(4):451–465, 2003.

[42] I. Banerjee and M. Ierapetritou. An adaptive reduction scheme to model reactive flow. *Combust. Flame*, 144(3):619–633, 2006.

[43] O. O. Oluwole, P. I. Barton, and W. Green. Obtaining accurate solutions using reduced chemical kinetic models: a new model reduction method for models rigorously validated over ranges. *Combust. Theor. Model.*, 11(1):127–146, 2007.

[44] K. He, M. G. Ierapetritou, and I. P. Androulakis. A graph-based approach to developing adaptive representations of complex reaction mechanisms. *Combust. Flame*, 155(4):585–604, 2008.

[45] H. Rabitz, M. Kramer, and D. Dacol. Sensitivity analysis in chemical kinetics. *Annu. Rev. Phys. Chem.*, 34:419–461, 1983.

[46] T. Turányi. Sensitivity analysis of complex kinetic systems. tools and applications. *J. Math. Chem.*, 5(3):203–248, 1990.

[47] T. Turányi. Reduction of large reaction mechanisms. *New J. Chem.*, 14(11):795–803, 1990.

[48] S. Vajda, P. Valko, and T. Turányi. Principal component analysis of kinetic models. *Int. J. Chem. Kinet.*, 17(1):55–81, 1985.

[49] S. Vajda and T. Turányi. Principal component analysis for reducing the Edelson-Field-Noyes model of the Belousov-Zhabotinsky reaction. *J. Phys. Chem.*, 90(8):1664–1670, 1986.

[50] H. Wang and M. Frenklach. Detailed reduction of reaction mechanisms for flame modeling. *Combust. Flame*, 87(3-4):365–370, 1991.

[51] M. Valorani, F. Creta, D. A. Goussis, J. Lee, and H. N. Najm. An automatic procedure for the simplification of chemical kinetic mechanisms based on CSP. *Combust. Flame*, 146(1-2):29–51, 2006.

[52] M. Valorani, F. Creta, F. Donato, H. N. Najm, and D. A. Goussis. Skeletal

mechanism generation and analysis for n-heptane with CSP. *Proc. Combust. Inst.*, 31:483–490, 2007.

[53] J. Prager, H. N. Najm, M. Valorani, and D. A. Goussis. Skeletal mechanism generation with CSP and validation for premixed n-heptane flames. *Proc. Combust. Inst.*, 32(1):509–517, 2009.

[54] T. Lu and C. K. Law. On the applicability of directed relation graphs to the reduction of reaction mechanisms. *Combust. Flame*, 146(3):472–483, 2006.

[55] T. Løvås, D. Nilsson, and F. Mauss. Automatic reduction procedure for chemical mechanisms applied to premixed methane/air flames. *Proc. Combust. Inst.*, 28:1809–1815, 2000.

[56] T. Løvås, P. Amnéus, F. Mauss, and E. Mastorakos. Comparison of automatic reduction procedures for ignition chemistry. *Proc. Combust. Inst.*, 29:1387–1393, 2002.

[57] T. Løvås. Automatic generation of skeletal mechanisms for ignition combustion based on level of importance analysis. *Combust. Flame*, 156(7):1348–1358, 2009.

[58] T. Lu and C. K. Law. A directed relation graph method for mechanism reduction. *Proc. Combust. Inst.*, 30:1333–1341, 2005.

[59] T. Zeuch, G. Moréac, S. S. Ahmed, and F. Mauss. A comprehensive skeletal mechanism for the oxidation of n-heptane generated by chemistry-guided reduction. *Combust. Flame*, 155(4):651–674, 2008.

[60] S. S. Ahmed, F. Mauß, G. Moréac, and T. Zeuch. A comprehensive and compact n-heptane oxidation model derived using chemical lumping. *Phys. Chem. Chem. Phys.*, 9(9):1107–1126, 2007.

[61] T. Nagy and T. Turányi. Reduction of very large reaction mechanisms using methods based on simulation error minimization. *Combust. Flame*, 156(2):417–428, 2009.

[62] T. Lu and C. K. Law. Linear time reduction of large kinetic mechanisms with directed relation graph: n-heptane and iso-octane. *Combust. Flame*, 144(1-2):24–36, 2006.

[63] X. L. Zheng, T. Lu, and C. K. Law. Experimental counterflow ignition temperatures and reaction mechanisms of 1,3-butadiene. *Proc. Combust. Inst.*, 31:367–375, 2007.

[64] T. Lu and C. K. Law. Strategies for mechanism reduction for large hydrocarbons: n-heptane. *Combust. Flame*, 154:153–163, 2008.

[65] P. Pepiot-Desjardins and H. Pitsch. An efficient error-propagation-based reduction method for large chemical kinetic mechanisms. *Combust. Flame*, 154(1-2):67–81, 2008.

[66] W. Sun, Z. Chen, X. Gou, and Y. Ju. A path flux analysis method for the reduction of chemical kinetic mechanisms. In *6th National Combustion Meeting*, number 23F3, May 2009.

[67] M. Raju, C.-J. Sung, and K. Kundu. Integrating sensitivity analysis into directed relation graph with error propagation for effective chemical mechanism reduction. In *Fall Technical Meeting of the Eastern States Section of the Combustion Institute*, number A-26, Sept. 2007.

[68] K. E. Niemeyer, M. Raju, and C.-J. Sung. Skeletal mechanism generation for surrogate fuels using directed relation graph with error propagation and sensitivity analysis. In *6th National Combustion Meeting*, number 11F1, May 2009.

[69] K. E. Niemeyer, M. P. Raju, and C.-J. Sung. Skeletal mechanism generation of surrogate fuels using directed relation graph with error propagation and sensitivity analysis. In *45th AIAA/ASME/SAE/ASEE Joint Propulsion Conference*, number AIAA 2009-5495, Aug. 2009.

[70] R. J. Kee, F. M. Rupley, E. Meeks, and J. A. Miller. CHEMKIN-III: A FORTRAN chemical kinetics package for the analysis of gas-phase chemical and plasma kinetics. Sandia National Laboratories Report No. SAND 96-8216, 1996.

[71] A. E. Lutz, R. J. Kee, and J. A. Miller. SENKIN: A FORTRAN Program for Predicting Homogeneous Gas Phase Chemical Kinetics with Sensitivity Analysis program for predicting homogeneous gas phase chemical kinetics with sensitivity analysis. Sandia National Laboratories Report No. SAND 87-8248, 1988.

[72] P. Pepiot and H. Pitsch. Systematic reduction of large chemical mechanisms. In *4th Joint Meeting of the U.S. Sections of the Combustion Institute*, number C17, Mar. 2005.

[73] L. Liang, J. Stevens, and J. T. Farrell. A dynamic adaptive chemistry scheme for reactive flow computations. *Proc. Combust. Inst.*, 32(1):527–534, 2009.

[74] L. Liang, J. G. Stevens, S. Raman, and J. T. Farrell. The use of dynamic adaptive chemistry in combustion simulation of gasoline surrogate fuels. *Combust. Flame*, 156(7):1493–1502, 2009.

[75] H. Curran, P. Gaffuri, W. Pitz, and C. K. Westbrook. A comprehensive modeling study of n-heptane oxidation. *Combust. Flame*, 114(1-2):149–177, 1998.

[76] H. Curran, P. Gaffuri, W. Pitz, and C. K. Westbrook. A comprehensive modeling study of iso-octane oxidation. *Combust. Flame*, 129(3):253–280, 2002.

[77] Y. X. Xin, C. K. Law, and T. F. Lu. A reduced mechanism for iso-octane oxidation. In *6th National Combustion Meeting*, number 23F5, May 2009.

[78] P. Glarborg, R. J. Kee, J. F. Grcar, and J. A. Miller. PSR: A FORTRAN program for modeling well-stirred reactors. Sandia National Laboratories Report No. SAND 86-8209, 1986.

[79] R. J. Kee, J. F. Grcar, M. D. Smooke, and J. A. Miller. A FORTRAN program for modeling steady laminar one-dimensional premixed flames. Sandia National Laboratories Report No. SAND 85-8240, 1985.

[80] T. Lu and C. K. Law. Diffusion coefficient reduction through species bundling. *Combust. Flame*, 148(3):117–126, 2007.

[81] T. Lu and C. K. Law. Systematic approach to obtain analytic solutions of quasi steady state species in reduced mechanisms. *J. Phys. Chem. A*, 110(49):13202–13208, 2006.